CHARACTERISTICS OF THE C-SO-164 RF ION SOURCE AND ITS PROPOSED CONVERSION TO MICROWAVE OPERATION

A Thesis

Submitted to the Faculty

of

Graduate Studies

The University of Manitoba

by

David A. Sawatzky

In Partial Fulfillment of the

Requirements for the Degree

of

Master of Science

Department of Physics

APRIL 1986 

ISBN 0-315-37447-0

CHARACTERISTICS OF THE C-SO-164 RF ION SOURCE AND ITS PROPOSED CONVERSION TO MICROWAVE OEPRATION

BY

DAVID A. SAWATZKY

A thesis submitted to the Faculty of Graduate Studies of the University of Manitoba in partial fulfillment of the requirements of the degree of

MASTER OF SCIENCE

ABSTRACT

The C-SO-164 is a radiofrequency ion source manufactured by High Voltage Engineering Corp. for use in a Van de Graaff accelerator. In the interest of inproving the C-SO-164's beam output and overall efficiency, an ion source test bed was constructed for measuring the source's beam current and emittance over a range of operating conditions. Design aspects are discussed for a modified version of the C-SO-164 in which the capacitively coupled RF electric field is replaced by a 2.45 GHz microwave field generated within a resonant cavity. A static magnetic field is used to induce electron cyclotron resonance and to concentrate the plasma near the exit canal. Because of the denser plasma and more efficient ionization attainable with microwave excitation, it is anticipated that the modified C-SO-164 will produce milliamps of proton current at a lower power and hydrogen consumption.

ACKNOWLEDGEMENTS

I would like very much to thank Vladimir Derenchuk and Iain Ritchie who acted as advisors for this project. Both gave very generously of their time, guidance, suggestions and advice. I would also like to thank Roger Dutton who made sure that funds were available for the project and that workshop items were processed quickly. A very special thanks to Lori Graham who spent many long hard hours typing this manuscript.

The experimental work was done at the University of Manitoba and was supported by Atomic Energy of Canada Limited.

TABLE OF CONTENTS

TABLE OF FIGURES

CHAPTER I

INTRODUCTION

1.1 Characteristics of Ion Sources

Throughout the brief history of ion source development, a primary goal has been to squeeze as much beam current as possible out of a source while maintaining a high ionization efficiency, low emittance, low cost, simplicity, and in some cases a high charge state. Such an ion source is, unfortunately, only in the imagination of the scientist, while in reality, practical ion source design is a game of tradeoffs. There is as yet no single general purpose ion source that is suitable for all applications and for this reason there is a large variety of different ion sources in use today. A source which is outstanding in one respect, say current output, will invariably suffer in some other aspect such as emittance, power consumption, or complexity of design. Selection or design of an ion source must be based on a few criteria which are of the most importance to the user. These must be determined by the application in which the source is to be used.

1.2 RF Sources in Van de Graaff Accelerators

Most single-ended Van de Graaff accelerators employ simple radio-frequency (RF) ion sources because they are light and rugged enough to withstand the mechanical stress and vibration to which they are subjected in the high voltage terminal. Also, because they do not have consumable electrodes, they require very little attention and servicing. This second feature is particularly important since gaining access to the source in a

single-ended Van de Graaff requires considerable dismantling of the machine, resulting in a significant amount of down time.

RF ion sources are normally used for production of light ions such as protons, deuterons, tritons, and alpha-particles. They are noted for their high beam currents (often hundreds of microamperes) and high ion yields (typically 90% pure for protons). Although RF sources do not generally consume much power (usually less than a kilowatt), they are fairly inefficient and only a small fraction of the input power is actually transmitted to the plasma while the remainder is expended through radiation and RF heating. This is an important consideration in a single-ended Van de Graaff accelerator since only a very limited supply of power is available from the alternator in the terminal.

The Whiteshell Nuclear Research Establishment (WNRE) operates a KN-4000 4.75 MV Van de Graaff accelerator manufactured by High Voltage Engineering Co. For the past several years the accelerator has been dedicated to the proton irradiation of zirconium alloy specimens which are subjected to a tensile stress. These experiments provide data which are useful in understanding the creep and growth in CANDU reactor pressure tubes which is influenced by the high neutron flux within the reactor. Up to now the experiments have required small proton currents (typically 5 μA at 4.5 MeV) which are easily provided by the C-SO-164 RF ion source which is currently installed in the accelerator. Future plans, however, point towards experiments requiring proton currents upwards of several hundred microamperes. This has prompted an analysis of the present ion source system to determine its capabilities and limitations, and to investigate possible improvements which would make the source better suited to high current output.

1.3 Objectives

The goal of this thesis is twofold. The first aim is to thoroughly bench test the C-SO-164 in order to gain a solid understanding of its operation and to determine its optimum operating conditions. This involved the construction of a vacuum chamber test bed with the necessary equipment for measuring beam current and emittance. Measurements of these characteristics over a wide range of operating parameters establishes a base against which the effectiveness of future modifications can be gauged.

The second objective is to investigate the feasibility of using microwaves to excite the plasma in the C-SO-164 instead of an RF electric field. The proposed system utilizes an inexpensive microwave oven magnetron with an operating frequency of 2.45 GHz to feed power into the plasma through a short section of tunable waveguide. Microwave excitation offers the advantages of more efficient ionization and a lower power consumption. Also, at microwave frequencies it becomes practical to enhance power transfer to the plasma with a static magnetic field of suitable strength to induce electron cyclotron resonance.

The modified proton source must, of course, be capable of functioning in the Van de Graaff high voltage terminal environment. This means that it must retain its gas cooling characteristics and be robust enough to withstand prolonged vibration.

Essentially, the development of the microwave source will be carried through the stages of fundamental design with preliminary tests and construction. The remaining phases of the project, including bench testing of microwave source and installation in the accelerator, are intended to be subject of a separate thesis.

CHAPTER II

THE RF ION SOURCE

2.1 History

The high frequency gas discharge was pioneered in the early 1930s by Rodebusch and Klingelhoeffer [1] for the production and study of chlorine atoms. Their apparatus consisted of a spherical glass vessel surrounded by a coil which was excited by a spark gap-type oscillator.

It was not until 1946, however, that Thoneman [2] first extracted a beam of positive hydrogen ions from an RF plasma. Using a 2 litre pyrex flask filled with hydrogen at a pressure of 10^{-3} Torr, the RF power was coupled in by means of two large ring-shaped electrodes outside of the flask. With an extraction probe voltage of 20 kV, he was able to produce an ion current of 10 mA. He later refined his source [3], replacing the flask by a 40 mm x 100 mm glass tube and by coupling the 20 MHz RF power into the tube through the use of an inductive coil. Using a probe voltage of 5 kV he was able to extract an ion current of 500 μA of which he estimated that 80 - 90% were protons. His source consumed hydrogen at a rate of 7.5 cc/hr.

In 1947, Bayly and Ward [4] developed an RF source employing a diaphram extraction technique in which the flat anode and extraction electrode are mounted close to each other in the base of the source, forming a Pierce-type system of ion optics. Using inductive coupling and a 1.2 kV extraction voltage, they were able to produce 500 μA of hydrogen ions with a gas consumption of 15 cc/hr.

A significant advance in the development of RF sources was the use of a static magnetic field to improve the ionization efficiency and reduce power consumption. In 1947 Ruthenglen and Cole [5] experimented with static magnetic fields as a means for improving the percent ion yield. In a source designed for use in a 1 MV accelerator they used two solenoid magnets to create an axial magnetic field of 130 Gauss. At a probe voltage of 2.8 kV they were able to extract 400 μA of current, of which over 64% was protons (their source yielded only 5% protons without the magnetic field). Their source consumed 30 W of power and 15 cc/hr of hydrogen.

Discovery of the resonance phenomenon in high frequency discharges (Koch and Neuert [6]) suggested that higher ionization efficiencies could be attained by the application of a transverse static magnetic field whose electron cyclotron frequency matched the excitation frequency. Mozorov [7] constructed an inductively coupled RF source which utilized a transverse static magnetic field provided by a permanent bar magnet. With a diaphram extraction voltage of 3 kV and a gas flow of 1.5 cc/hr, Mozorov's source produced 100 μA of beam current.

Transverse magnetic fields have not been used to a large degree in RF sources because, unlike the axial magnetic field, they do nothing to prevent the diffusion of electrons and ions to the walls of the bottle. They did, however, point the way toward the development of electron cyclotron resonance (ECR) sources which have become very widely used since the late 1970s.

2.2 Principles of Operation

The RF ion source employs a radiofrequency electric field to provide electron heating which in turn causes ionization of gas molecules, producing a plasma from which an ion beam can be extracted. As with most types of ion

sources, there are many variations of the RF source all working on the same fundamental principles.

Most RF ion sources operate in the 10 - 100 MHz frequency range with a gas pressure of 10^{-2} to 10^{-3} Torr. Typically, an RF source will consist of a pyrex or quartz bottle into which a gas is admitted (Figure 2.1). RF power provided by an oscillator circuit is coupled into the bottle either capacitively or inductively. In capacitive or "direct" coupling, two ring-shaped electrodes encircle the bottle and the RF voltage across the electrodes produces an RF field between them. Inductive coupling utilizes a coil of perhaps 6 to 10 turns around the bottle to create an alternating magnetic field within it. The magnetic field in turn induces an alternating electric field inside the bottle.

Whether generated directly or inductively, the high frequency electric field will cause any free electrons to be accelerated back and forth. As they oscillate they will collide with gas molecules, ionizing them to produce a plasma consisting mostly of positive ions, electrons, neutral molecules and atoms in various excited states. In general, it has been found [7] that electric field excitation by capactive coupling will create a plasma at a lower gas pressure (as low as 10^{-5} Torr) than by inductive coupling.

At the low pressures at which RF ion sources are typically operated, free electrons are created predominantly by secondary emission from the walls of the discharge chamber. For this reason, the source bottle must be made from a material with a secondary emission coefficient $\delta > 1$ so that enough free electrons can be generated to ignite a plasma.

The most commonly used technique for extracting ions from the plasma is the "probe extraction" method. This method uses a large positive potential applied to the probe electrode (Figure 2.1) in the end of the source bottle to

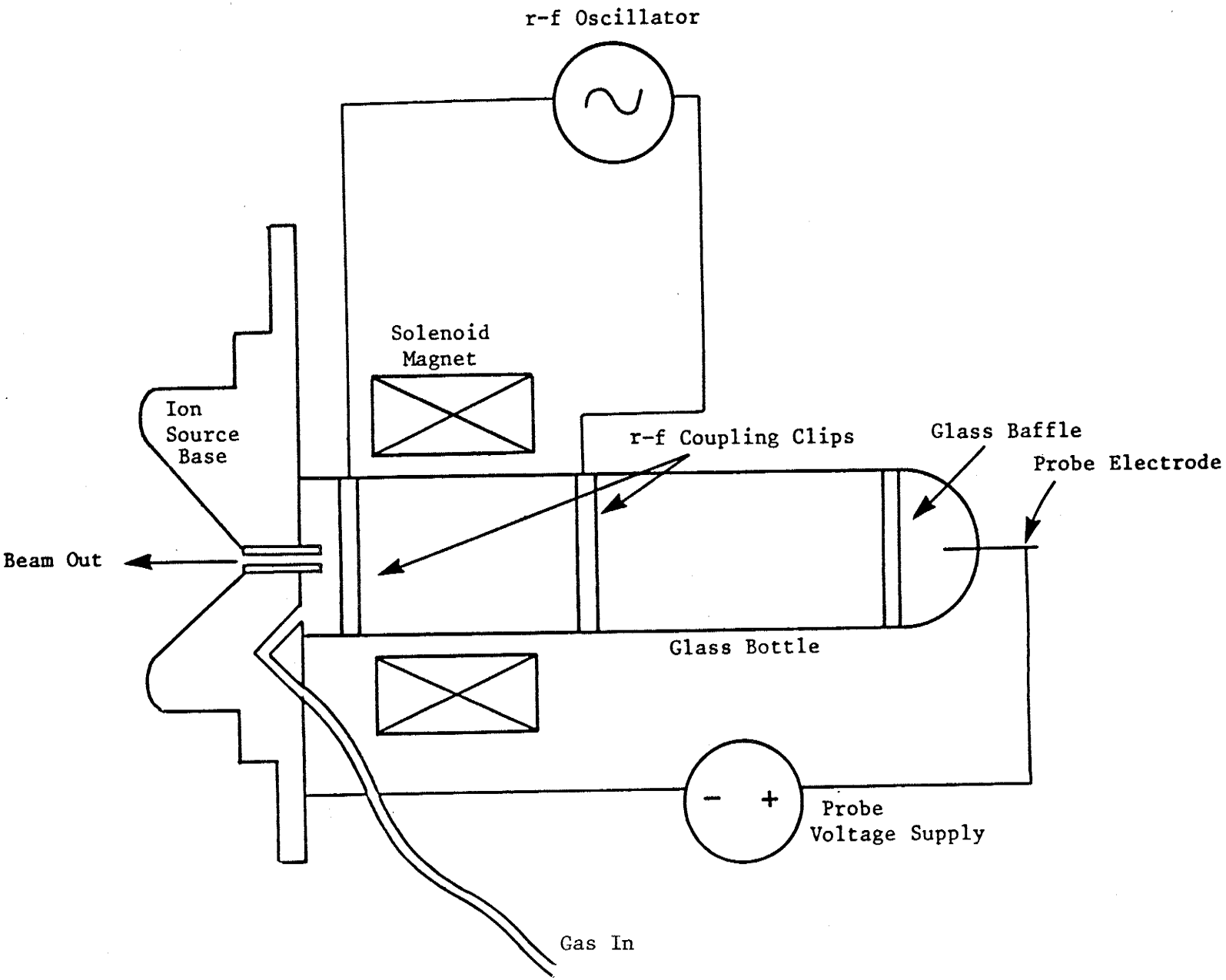

Figure 2.1 The RF Ion Source

create a static electric field, which drives the positive ions out of the bottle via the exit canal. The probe electrode must be protected from the high energy electrons which are accelerated back towards it by the static electric field. At the same time, the probe must remain exposed to the discharge in order to remove free electrons at the same rate that positive ions leave the bottle. This is necessary to maintain the overall charge neutrality of the plasma. Electrode protection is usually provided by a glass baffle (Figure 2.1) or by a constriction in the source bottle.

The static axial magnetic field produced by the solenoid coil encircling the bottle (Figure 2.1) serves to improve the ion yield by increasing the lifetime of the free electrons. The electrons tend to spiral along the magnetic flux lines which cause them to travel essentially along the axis of the bottle, away from the walls. Similarly, it prevents the ions from diffusing to the walls thereby lowering the recombination rate. The magnet is usually positioned so as to concentrate the plasma in the region near the exit canal.

The primary reason why RF sources have such a high percentage ion yield is because of the low recombination rate. The source bottle is made of glass or quartz with a low recombination coefficient, and with the RF electrodes mounted external to the bottle there is no metal surface in contact with the plasma aside from the tiny extraction probe. As a result, very little recombination takes place at the walls and so most of the ions are able to survive long enough to ionize completely. Recombination with other gas molecules and ions is also minimized by keeping the gas pressure low.

2.3 The RF Dishcarge

2.3.1 Mechanisms of Plasma Production

In order to produce a plasma that is rich in a particular ion species, molecular dissociation involving many mechanisms must take place, not all of which are well understood. There is seldom a single process by which a molecule dissociates. More usually it occurs though a seemingly random series of reactions. At any given moment there are likely to be many different chemical and atomic processes occurring simultaneously in a plasma.

The process by which protons are produced from hydrogen is divided into two stages of ionization which are characterized by the different colors of light emitted by their plasmas. The first stage consists of the reactions due to the initial collision of an electron with a hydrogen molecule. The presence of the first stage reactions listed below can be identified by a pale greenish white glow from the plasma.

First Stage:

$$H_2 + e \rightarrow H_2^+ + 2e$$

$$H_2 + e \rightarrow H^+ + H^- + e$$

$$H_2 + e \rightarrow H + H + e$$

The second stage is made up of the reactions that occur with the byproducts of the first stage. It is characterized by a bright reddish-pink color. The predominant second stage reactions are listed below.

Second Stage:

$$H_2^+ + e \rightarrow H^+ + H^-$$

$$H^- + e \rightarrow H + 2e$$

$$H_2^+ + e \rightarrow H^* + H^*$$

$$H^+ + H^- \rightarrow H^* + H^*$$

$$H_2^+ + H^- \rightarrow H^* + H^* + H^*$$

$$H^+ + e \rightarrow H^*$$

The H* represent hydrogen atoms in an excited state and the radiative decay of the orbiting electron is responsible for the photon emission that produces the reddish-pink glow.

The color of the plasma is usually a good indicator of its condition. Early experiments by Ruthenglen and Cole [5] showed that a bright reddish plasma indicates more than 50% protons in the emergent beam, while a steely blue color indicates less than 20% protons. A dull pinkish glow is associated with the presence of air molecules in the plasma and is often observable when there is a leak or after the inside of the source has been exposed to atmosphere.

2.3.2 Electron Motion*

Under the influence of the applied RF electric field, the free electrons in the plasma oscillate at the same frequency as the RF field. As long as the electrons continue to oscillate without collision there is no net energy transfer from the RF field. When the electrons begin to collide with the gas particles, there will be some power transfer into the discharge region, but it will not contribute to ionization unless the electron energy E_e equals or exceeds the ionization energy E_i which is 15.4 eV in the case of an H_2 molecule. This means that the electron mean free path λ_e must be large enough that an electron can be accelerated to a velocity

$$v_e \geq \sqrt{\frac{2}{m_e}} E_i \qquad (2.3.1)$$

where m_e is the electron mass. The implication of equation (2.3.1) is that too high a gas pressure in the source bottle can reduce the electron mean free path to a point below which sufficient velocity cannot be attained to produce an ionizing collision.

* This section is based on the treatment of the problem by Valyi [T1].

If one considers a plasma in the absence of an external electric field, the average electron velocity in a given direction will be zero ($\langle v_e \rangle = 0$). If we impose an electric field E on the plasma, the electrons will acquire a net drift velocity in the direction of the field. The average electron velocity is determined by

$$\frac{d\langle v_e \rangle}{dt} = \frac{-eE}{m_e} \tag{2.3.2}$$

From equation (2.3.2) it appears that for E constant, an electron is continuously accelerated. In actual fact, the collisions between the electrons and the heavier particles create a resistive force which opposes the accelerating force, eventually causing the electron to attain an equilibrium velocity.

The probability that an electron will collide with a more massive particle in the small time interval, dt, is given by dt/τ, where τ is a constant with the units of time. It is assumed that in each collision the electron loses all the energy that it has gained from the external field and that its velocity after the collision is entirely random. Since the probability of collision per unit is $1/\tau$, the rate of change of $\langle v_e \rangle$ due to collisions is given by

$$\left(\frac{\partial\langle v_e \rangle}{\delta t}\right)_{\text{collision}} = - \frac{\langle v_e \rangle}{\tau} \tag{2.3.3}$$

From equation (2.3.2) it is seen that the acceleration due to the external field is

$$\left(\frac{\partial\langle v_e \rangle}{\delta t}\right)_{\text{field}} = - \frac{eE}{m_e} \tag{2.3.4}$$

The equation of motion for the electron is therefore,

$$m_e \frac{d\langle v_e \rangle}{dt} = - eE - \frac{m_e \langle v_e \rangle}{\tau} \tag{2.3.5}$$

It can be shown statistically that τ is in fact the mean time between collisions. If we simply call the average electron velocity v_e, then the equation of motion can be written as

$$m_e \frac{dv_e}{dt} + m_e \nu v_e = eE \tag{2.3.6}$$

where the collision frequency $\nu = \tau^{-1}$.

If the applied electric field is given by $E = E_o \cos \omega t$ then the solution of equation (2.3.6) yields the following expression for average electron velocity.

$$v_e = \frac{eE_o}{m_e(\nu^2 + \omega^2)^{1/2}} \sin(\omega t + \phi) - Ce^{-\nu t} \tag{2.3.7}$$

where $\phi = \arctan(\nu/\omega)$ and C is an integration constant. From equation (2.3.7) it can be seen that over a long period of time the electron's motion is sinusoidal. The fact that the electron's oscillations are out of phase with the RF field indicates that the electron is removing power from the RF field and delivering it to the discharge.

2.3.3 Power Transfer

The electron current density per unit volume is given by the expression

$$j = n_e e v_e \tag{2.3.8}$$

where n_e is the electron concentration. The average power dissipation per unit volume is

$$P = \frac{1}{t} \int_o^t j \cdot F \, dt \tag{2.3.9}$$

where F is the RF electric field. Inserting (2.3.7) and (2.3.8) into (2.3.9) and assuming $t \gg 1$, the result of the integration is

$$P = \frac{n_e e^2 E_o^2 \nu}{m_e(\nu^2 + \omega^2)} \qquad (2.3.10)$$

It is apparent from equation (2.3.10) that the power transmitted from the electrons to the discharge is directly proportional to the electron concentration. This is not surprising since, on the average, each electron delivers the same amount of energy to the discharge. The power is also proportional to the square of the electric field strength, E_o. It is evident from (2.3.10) that an increase in the RF frequency ω, results in a decrease in power, unless it is accompanied by a corresponding increase in the field strength. Increasing the frequency means that the electron is accelerated over a shorter period of time thereby decreasing the distance travelled during each oscillation. As a result, fewer collisions occur and the power transfer decreases. Notice also that when the collision frequency $\nu = 0$, then the power $P = 0$ as well, verifying that collisions must occur if a net energy transfer from the RF field is to take place.

By taking the derivative of equation (2.3.10) with respect to ν and equating the result to zero, it can be seen that for a given RF frequency ω, the power transfer is maximized when $\nu = \omega$. The implication of this is that for a particular RF frequency there exists an optimum gas pressure for which the energy transfer is most efficient. Operating experience with the C-SO-164 has indicated that there is, in fact, an optimum pressure for which the beam current is maximized, all other parameters remaining unchanged. This would imply that the power transfer is optimized at that pressure, due to resonance.

CHAPTER III

THE ION SOURCE TEST BED

3.1 The C-SO-164

The C-SO-164 is a radiofrequency, positive ion source manufactured by High Voltage Engineering Corporation (HVEC) for use in their Van de Graaff accelerators. The source is rated for a maximum proton current of about one milliampere. The C-SO-164 (shown in Figure 3.1) employs capacitve RF coupling and a probe extraction. Gas is admitted into the pyrex source bottle via the ion source base, which is specifically designed to fit the flange of a HVEC accelerator tube. The quartz exit canal in the source base has an inner diameter of 2 mm.

The tuning capacitor is used to maximize power transfer from the oscillator to the plasma (the capacitor was not used in the experimental test set-up). The solenoid magnet that comes with the C-SO-164 is a sealed unit that snaps on to the ion source base. Since such a magnet was not available for experimental purposes, an ORTEC model 305 magnet coil of similar specifications was used.

The C-SO-164 is designed to be cooled by the circulation of the pressurized sulfur hexafluoride insulating gas which fills the tank of the Van de Graaff accelerator. The source must be forced air cooled when operating in atmosphere.

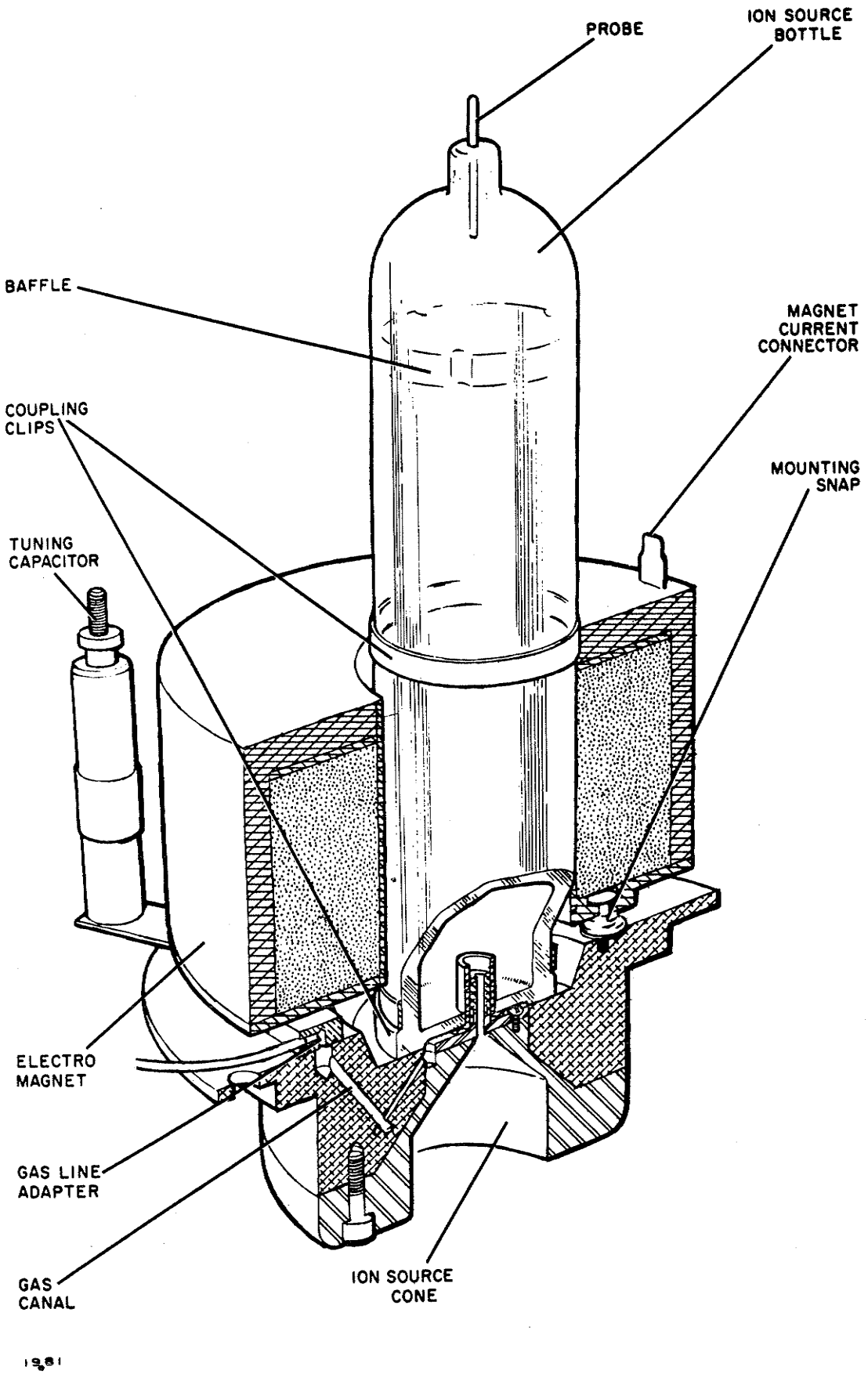

Figure 3.1 The C-SO-164

3.2 Power Supplies

The power supplies for the C-SO-164 are all custom built to reside in the terminal of the KN-4000 Van de Graaff accelerator. They are designed to be run with an input voltage of 120 Vac at a frequency of 400 Hz. Since these supplies were not suitable for use outside of the accelerator, the power supplies and oscillator from an ORTEC model 501 RF ion source were used for operating the C-SO-164 on the test bed. The 501 is a general purpose RF source with operating characteristics very similar to those of the C-SO-164. As a result, all of its associated power supplies are suitable for use with the C-SO-164.

The RF oscillator is an ORTEC model 307 which generates 80 W of RF power at a frequency of 80 MHz. Clip leads from the oscillator coil connect directly to the RF coupling electrodes. The model 308 dc power supply is a separate unit which provides plate and grid voltage and filament currents for the two 8072 tetrodes in the oscillator. The probe voltage is generated by an ORTEC model 309 dc power supply. The 309, which is rated at a maximum voltage of 6 kV, is unregulated and so the output voltage level is controlled by means of a variac on the power input. A model 304 dc power supply provides the solenoid magnet with a current ranging from zero to one ampere. The current output is also controlled by a variac on the power input.

3.3 Vacuum System

The C-SO-164 is mounted on a vacuum chamber which is maintained at a low pressure to permit operation of the source and passage of the emergent beam. Figures 3.2 and 3.3 illustrate the construction of the vacuum chamber. For clarity, the supporting structure, roughing pump, and the cage surrounding the source to reduce RF radiation are omitted from the diagrams. Essentially, the

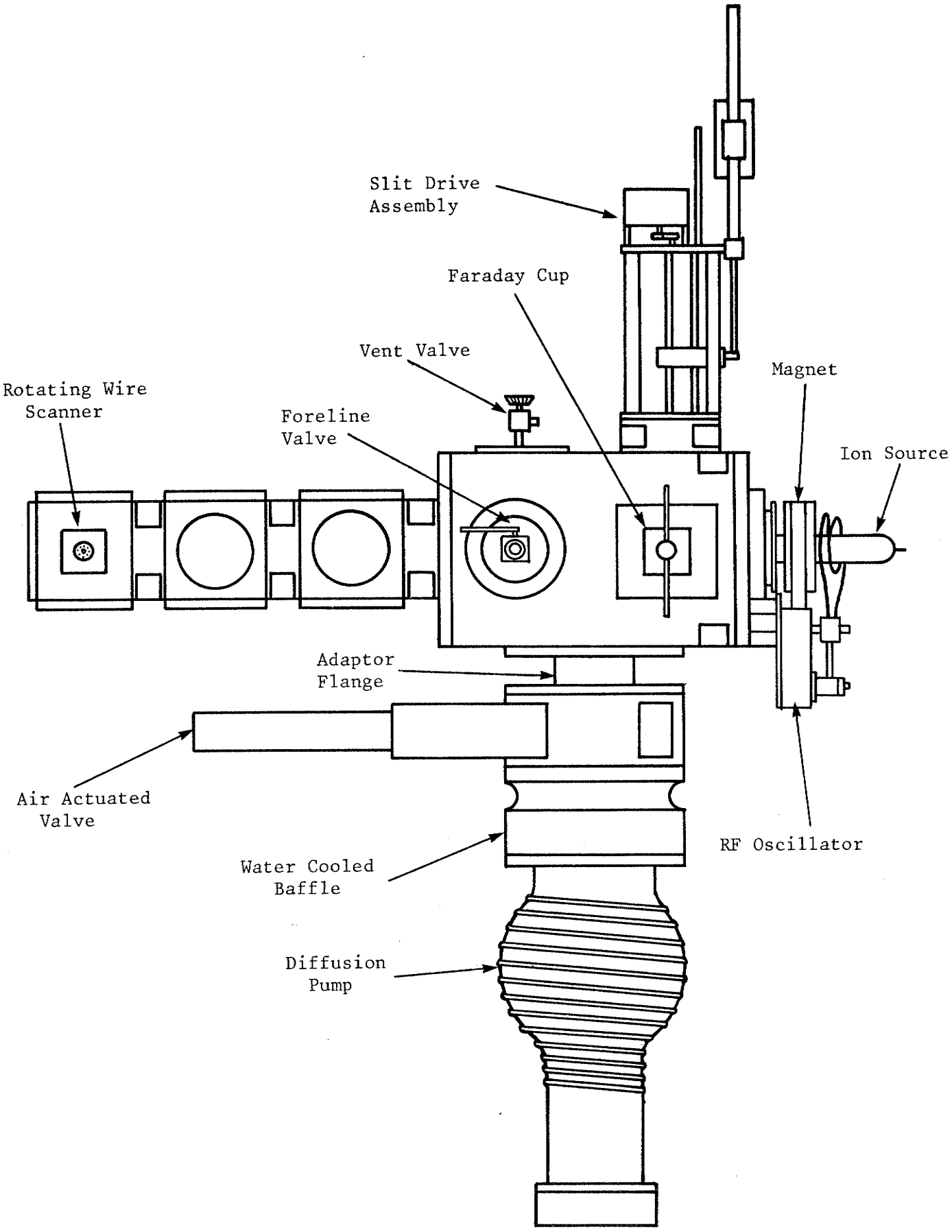

Figure 3.2 Vacuum Chamber (side)

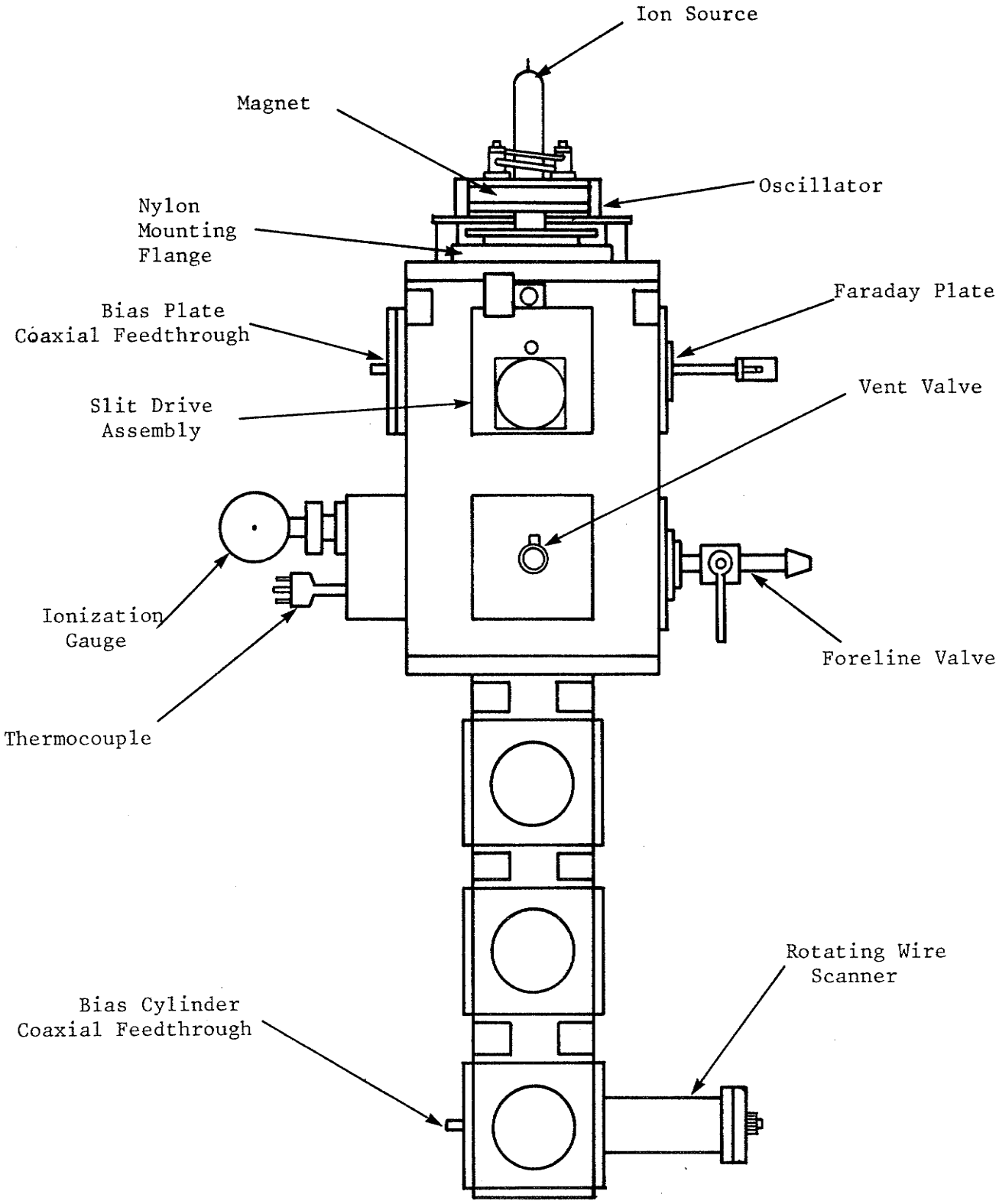

Figure 3.3 Vacuum Chamber (top)

test bed is constructed from aluminum parts and consists primarily of a box-shaped vacuum chamber with the ion source mounted on one end and a beamline extension on the other end.

Pumping is provided by a Varian VHS-6 diffusion pump along with a Sargent-Welch model 1376 forepump. The forepump was also used to rough the vacuum chamber down to 10 microns before opening it to the diffusion pump by means of the isolation gate valve. An air actuated gate valve and a water-cooled baffle are located just above the diffusion pump. With the valve and baffle in place, the system has a pumping speed of 1200 ℓ/s for air. All flanges are sealed with BUNA-N O-rings and pressure is monitored by means of a thermocouple gauge and ion gauge mounted on the side of the vacuum chamber, as well as a thermocouple gauge on the pump foreline. Pressure in the vacuum chamber is typically around 1.5×10^{-6} torr when there is no gas flow to the ion source. Gas flow to the source is regulated by a needle valve.

The ion source is mounted on a nylon insulating flange so that the entire ion source assembly can be floated at high voltage, permitting operation with a focussing electrode maintained at ground potential. No focussing was used, however, for any of the experiments conducted for this thesis, and so the ion source base was kept at ground potential.

3.4 The Slit

A 1 mm wide movable slit, located 8 cm from the source base, was used for making emittance measurements. The slit assembly (Figure 3.4) is constructed from a piece of copper plate with a circular hole in it. Two pieces of straight-edged aluminum foil are epoxied to the back of the plate with a separation of 1 mm to form the slit opening. A short 10-24 stud, fixed to one side of the plate permits the slit assembly to be screwed into the

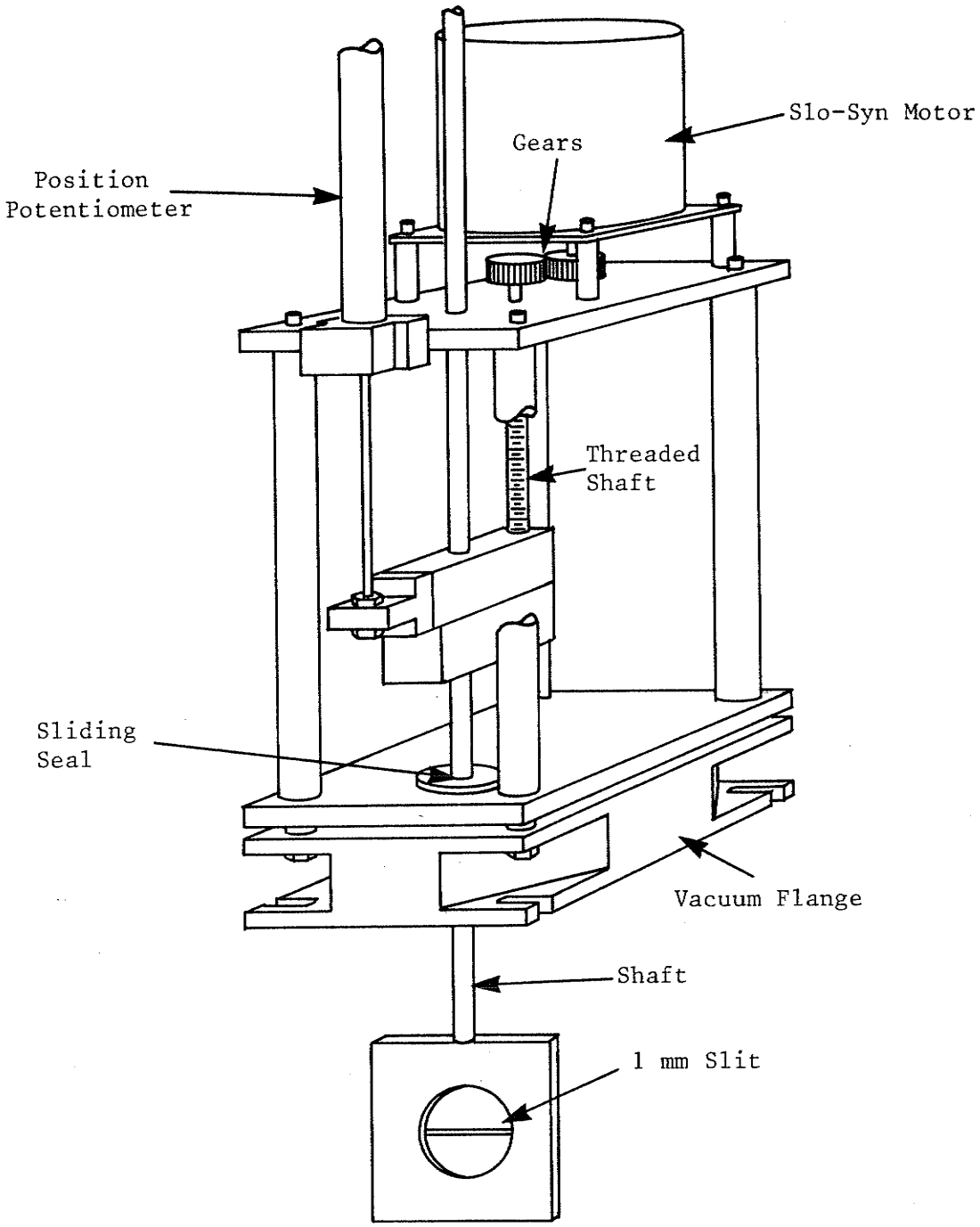

Figure 3.4 The Slit

tapped end of a movable shaft. The slit drive assembly (Figure 3.4) uses a SLO-SYN motor turning a threaded shaft to move the slit back and forth within the vacuum chamber.

Movable microswitches set the travel limits of the slit, while a simple SLO-SYN control unit is used to drive the motor. A high precision potentiometer provides a calibrated voltage output directly proportional to the slit position.

3.5 The Faraday Plate

The "Faraday plate" is a term coined to describe the device which is used to measure the beam current of the ion source. The Faraday plate (Figure 3.5) is located about 10 cm from the ion source base. It consists of an aluminum plate mounted on a sliding stainless steel shaft which permits the plate to be manually moved in and out of the beam. The shaft, which contains two copper tubes for water cooling of the plate, is insulated from the vacuum chamber by a nylon guide and rubber O-ring. A copper plate with circular hole is supported by ceramic spacers just off the front face of the Faraday plate. The copper plate is biased at a potential of about -200 V in order to repel secondary electrons back onto the Faraday plate. The alligator clip on the copper water cooling tube connects the Faraday plate to the BNC connector. The Faraday plate is grounded through a sensitive current to voltage convertor. Therefore, any beam current striking the plate will pass through the convertor producing a proportional voltage which can be read on a digital voltmeter.

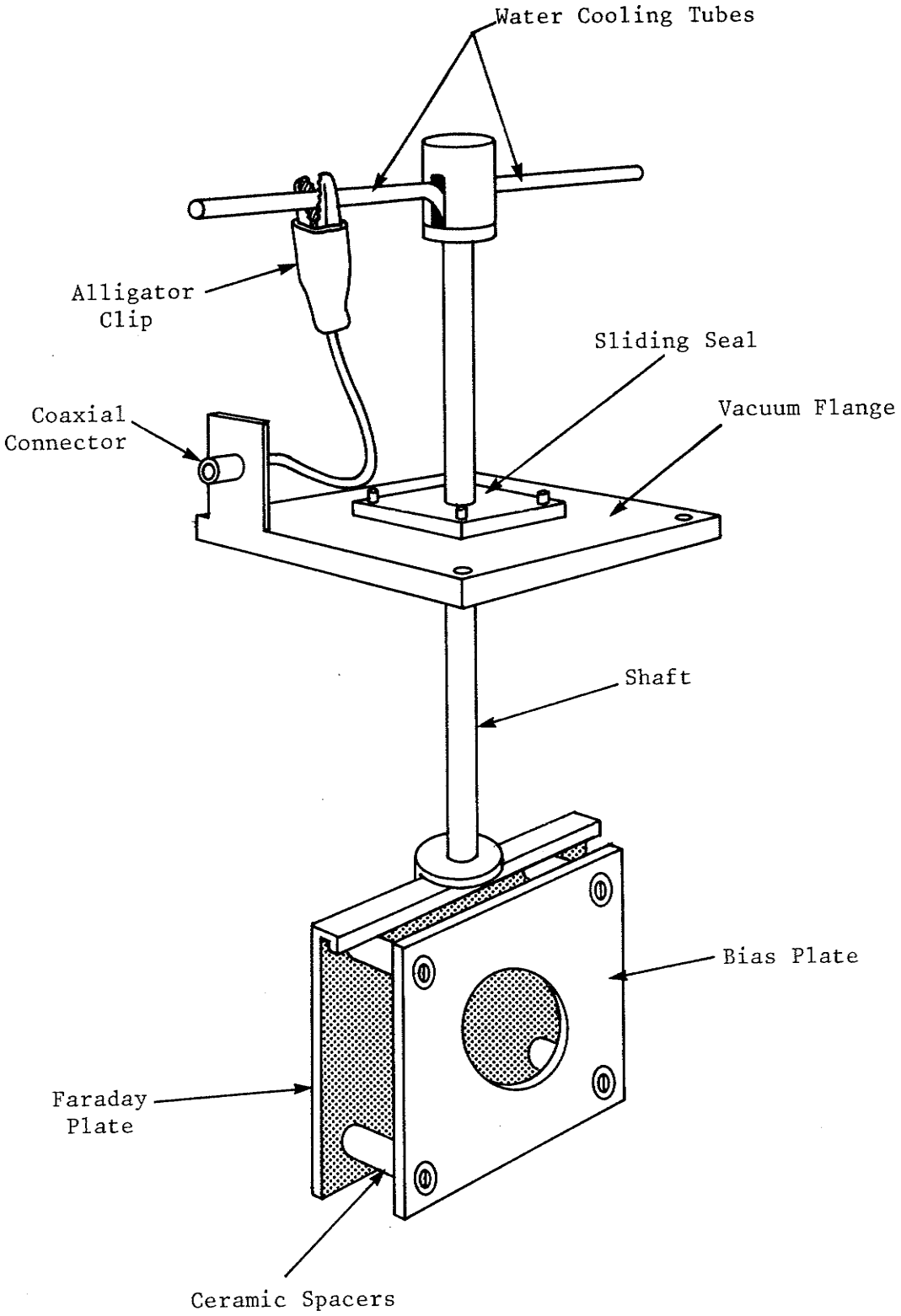

Figure 3.5 Faraday Plate

3.6 The Scanner

A rotating wire scanner located 90 cm from the source base provides a cross-sectional profile of the proton beam. It is used in conjunction with the slit to perform emittance measurements. Figure 3.6 illustrates the construction of the scanner. A piece of steel wire is mounted on the end of a rotating brass arm which is driven by a small dc motor. The wire and arm are insulated from the vacuum chamber and a small metal brush which is in contact with the rotating shaft to electrically connect the wire to the 8 pin connector on the top of the device. The rotating wire is grounded through a current sensitive amplifier so that, as the wire passes through the beam, it produces a voltage signal proportional to the beam current, which can be observed on an oscilloscope.

The cylinder shown in Figure 3.6 is placed over the rotating wire. Biased at a potential of 100 V, the cylinder removes all secondary electrons which are knocked off of the wire, while permitting the higher energy protons to pass straight through. The microswitches are used to provide a position reference for triggering the oscilloscope or device that is monitoring the scanner.

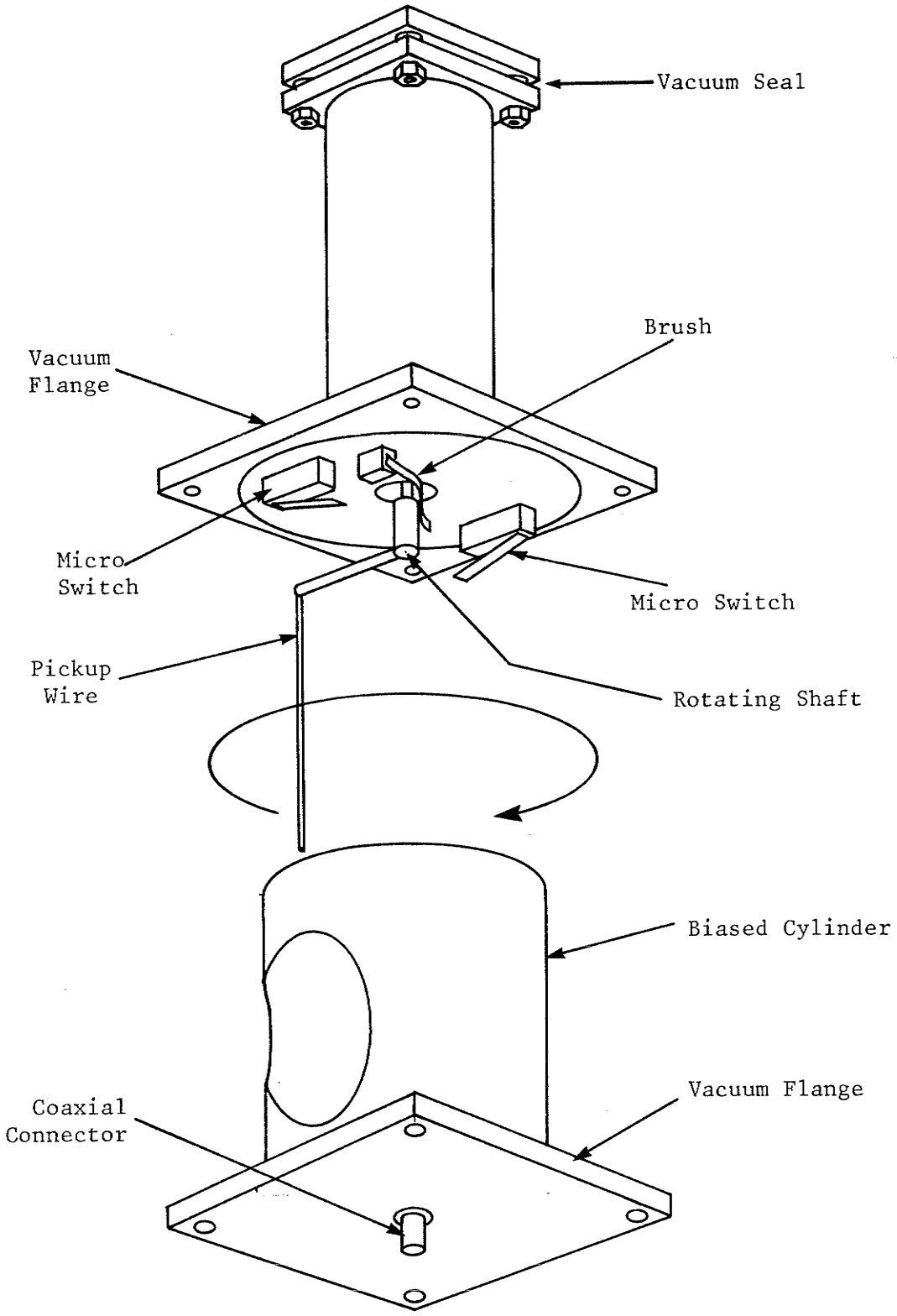

Figure 3.6 Scanner

CHAPTER IV

EMITTANCE MEASUREMENT

4.1 Emittance

Emittance is the analytical tool used to characterize an imperfect particle beam. If it were possible in practice to produce a beam of particles with perfectly parallel trajectories, then there would be no need to define an emittance. Unfortunately, in any real ion beam there will be a variation of trajectories at any point. The beam cannot be described as laminar flow, because particle paths are continuously crossing each other. This dispersion in transverse velocity can result from the initial thermal velocities of the ions or from any subsequent aberration introduced into the beam.

Each ion trajectory can be characterized in one dimension by a pair of parameters (the transverse slope or momentum and the transverse position). These parameters represent a point in phase (r', r) space. A certain fraction of the trajectories, within a beam of particles at some chosen position, will be contained within a closed curve in phase space. This closed curve is usually assumed to be an ellipse, although in practice it is often found to be irregular in shape. Because of the Gaussian nature of the beam profile, there cannot exist an actual curve which encompasses all of the rays. The boundary is usually defined as a normalized brightness contour, containing an arbitrary percentage of the beam's total intensity.

In three-dimensional cartesian space, a beam with a central reference trajectory along the z axis would have two separate phase space plots defining its emittance in the x and y planes. The actual emittance is usually defined

as the area of the closed curve in r-r' phase space divided by π. It is proportional to the inverse square root of the beam energy. By virtue of Liouville's theorem, the emittance of a beam is an invariant quantity and will remain constant along the path of the beam as long as the particle energies do not change. Since the area of the phase space ellipse changes only as a function of the square root of the particle energies, the emittance is often normalized with respect to the energy.

4.2 Measurement Technique

There are a variety of different methods [8-16] that have been used for measuring the emittance of ion beams. The technique employed in this thesis utilizes a movable slit and a beam profile monitor. The theory behind this method is quite straightforward. The slit (Figure 4.1(a)) defines the transverse position, r_o, of the beam slice that is being analyzed. The current density distribution of the beam slice is essentially Gaussian and its amplitude is normalized with respect to the peak current found in the beam. This normalized current is referred to as "brightness".

The transverse dispersion of the beam slice at displacement r_o is represented by the width of the current pulse at a level corresponding to an arbitrary brightness. Figures 4.1(a) and (b) show how these points are transformed into r-r' phase space for the cases of 25% and 50% brightness contours. The complete contours are obtained by plotting these points over the entire range of slit movement.

For measuring the emittance of a beam, the brightness contour is normally defined to contain as large a percentage of the total beam as is practically possible (typically 90-95%). The lower percentage contours are useful, as well, in showing the beam's intensity distribution.

Obtaining the divergence angle, r', of a particular ray using the rotating wire scanner requires a simple calculation. Notice that the ray in Figure 4.2 intercepts the cylinder circumscribed by the rotating wire at two

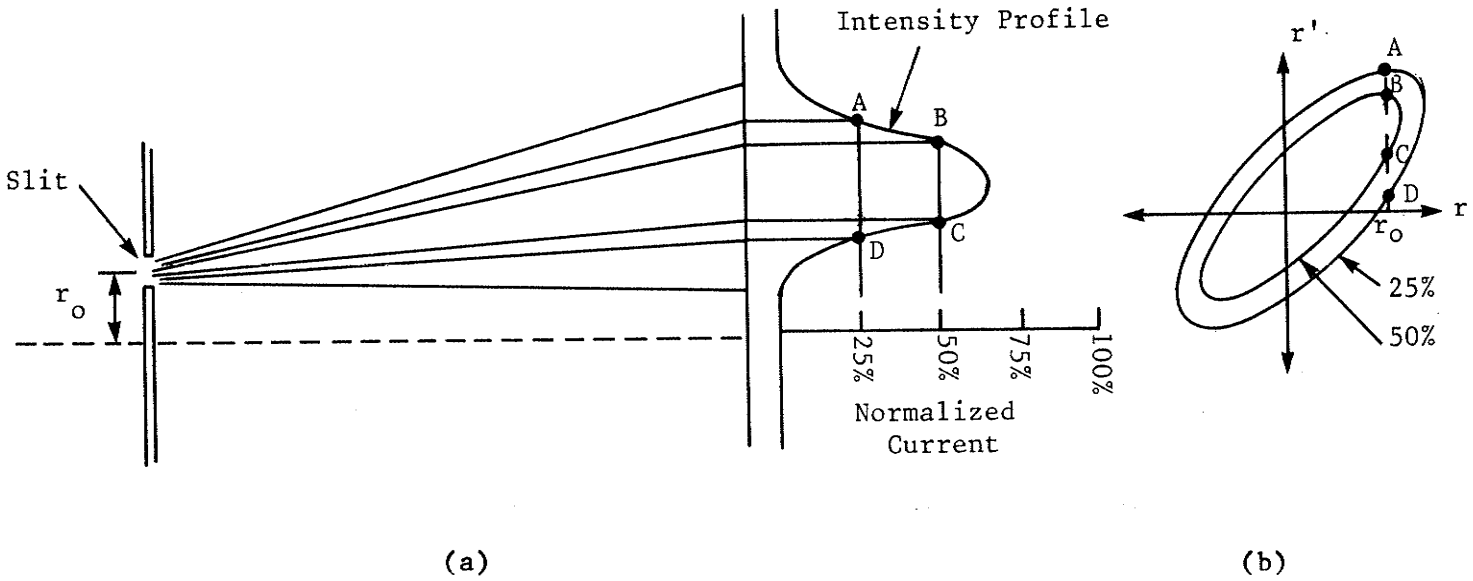

(a) (b)

Figure 4.1 Measurement of Brightness Contours

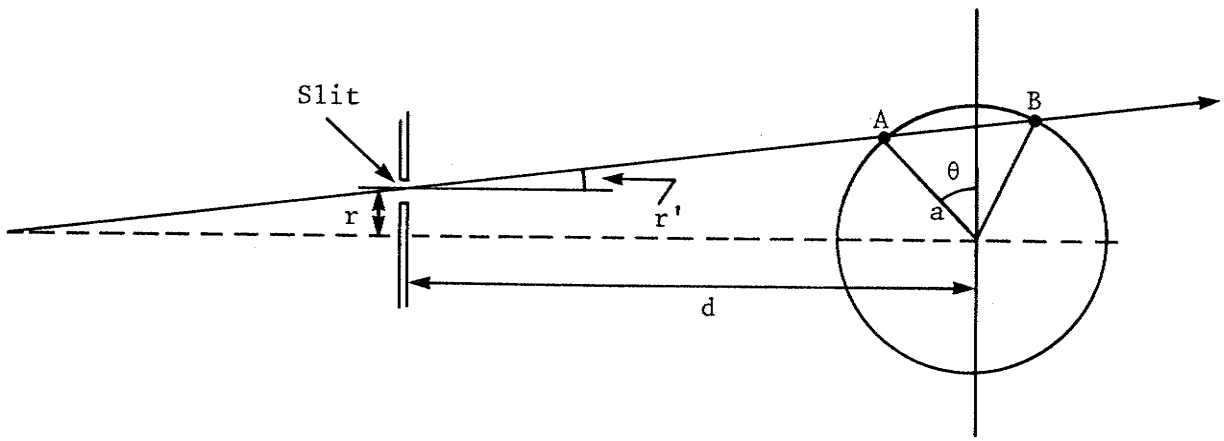

Figure 4.2 Scanner Operation

separate points. Either of these points A or B may be used to find the divergence angle r'. If the arm on which the wire is mounted has a length a and forms an angle θ with a line perpendicular to the beam axis, then the divergence angle r' is given by the expression

$$r' = \arctan \left\{ \frac{a \cos\theta - r}{d - a \sin\theta} \right\} \qquad (4.2.1)$$

Since the wire rotates at an angular frequency ω,

$$\theta = \omega t \qquad (4.2.2)$$

where t is the time. Substituting the above expression into equation (4.2.1) yields a divergence angle r' of

$$r' = \arctan \left\{ \frac{a \cos\omega t - r}{d - a \sin\omega t} \right\} \qquad (4.2.3)$$

Using equation (4.2.3), the time axis of each beam profile plot can be redefined in radians, representing the divergence angle r'.

4.3 Equipment

Figure 4.3 is a block diagram showing the configuration of the various pieces of equipment that were used for collecting the emittance data. The scanner (described in section 3.6) was driven at a frequency of approximately 0.2 Hz. In early experiments there was found to be a severe problem with low frequency noise of amplitude comparable to the beam signal. The noise was eventually traced to the dc motor which drives the scanner. The arcing of the brush contacts and alternating magnetic fields within the motor were inducing small currents in the motor shaft which superimposed onto the beam signal. The problem was rectified by insulating the scanner wire from the motor shaft.

The beam current signal from the scanner is delivered via coaxial cable into a current to voltage convertor which was built by modifying the amplifier circuit of an old integrator unit. The current input to voltage output ratio of the unit is 1 μA to 100 mV and its circuit diagram is shown in Appendix A.

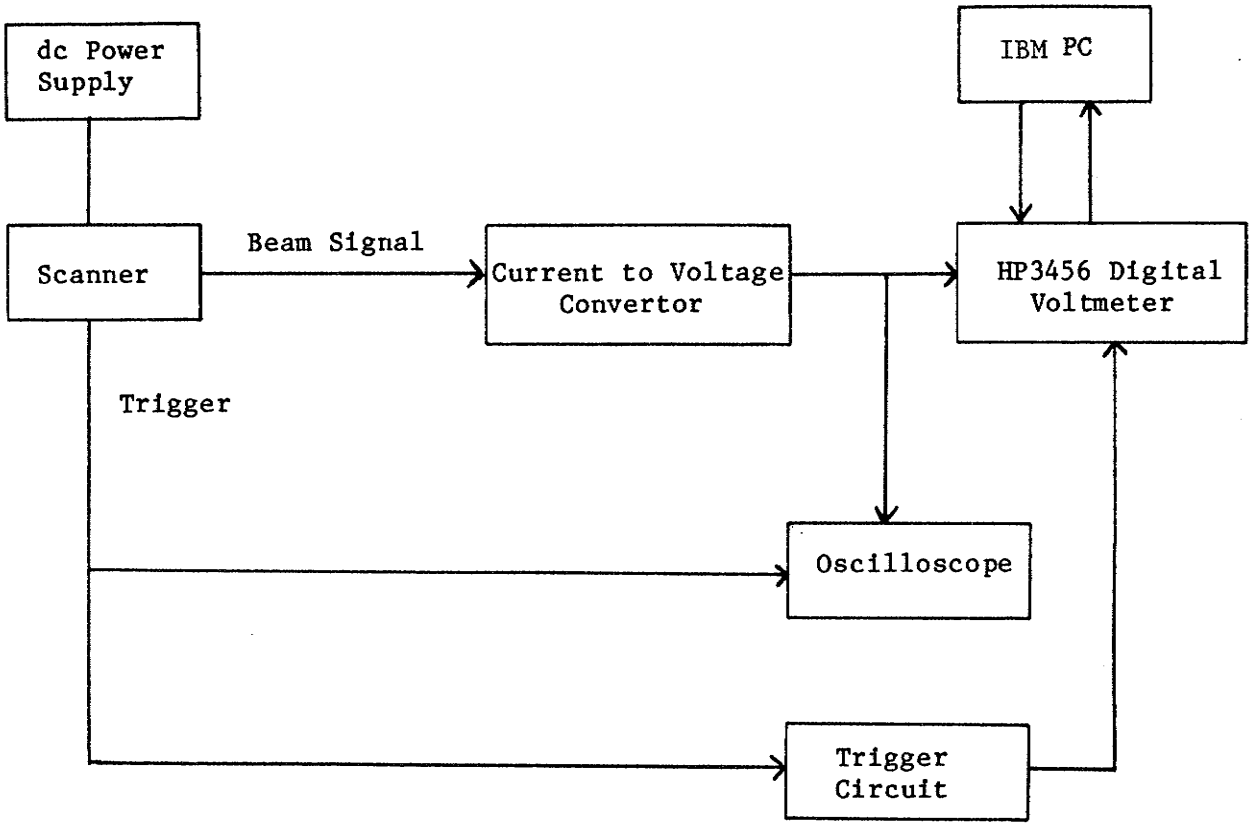

Equipment Configuration

Figure 4.3

The output from the current to voltage convertor goes to an oscilloscope and also to a Hewlett Packard HP3456 digital voltmeter. The HP3456 is a programmable voltmeter which has the capability to take bursts of readings and to store them in internal memory. The HP3456 was programmed to collect and store 300 readings over a period of two scanner revolutions.

Triggering of the oscilloscope and HP3456 was achieved with a microswitch in the scanner (Figure 3.6), activated by the brass arm supporting the rotating wire. Of the two microswitches mounted on the scanner, only one was required to establish the starting point of each scan and that microswitch was adjusted such that it would be depressed on initial contact with the rotating arm and released when the scanner arm is exactly perpendicular to the beam axis. The signal going into the microswitch comes from the dc power ($\sim$ 1 V) which drives the scanner motor. The trigger signal coming from the scanner, therefore, is a pulse with amplitude of approximately 1 V and a duration of about 1/5 second (the time during which the microswitch is closed).

Although this signal is sufficient for triggering the oscilloscope, it is not suitable for triggering the HP3456 which triggers on a TTL level negative edge transition. To meet this requirement, a special triggering circuit was designed and built to debounce the signal from the microswitch, and on detection of its negative edge to emit a TTL negative pulse of 0.5 μsec duration for the HP3456. In addition, the circuit locks out any subsequent triggering pulses until a reset switch has been depressed. This prevents the HP3456 from being interrupted by a trigger pulse while collecting a burst of readings. Further information on the triggering circuit, as well as diagrams are found in Appendix A.

The HP3456 was interfaced to an IBM personal computer by means of an National Instruments GPIB-PC interface board. Its accompanying software

routines allow the computer to exchange data with the HP3456. Essentially, the computer was used to set the HP3456's operating parameters and, after each burst of readings, to dump the contents of its internal memory on to floppy disk. In this manner, a series of emittance beam profiles are stored in data files on floppy disk. They are later transferred to a Vax 11/750 on which they are processed and plotted.

CHAPTER V

CHARACTERISTICS OF THE C-SO-164

5.1 Beam Current

The beam current extracted from the C-SO-164 is found to be dependent on a number of variable parameters. These include extraction probe voltage, magnetic field, and gas pressure. The extraction probe voltage can be varied over a range of 0 to 6 kV. The C-SO-164 is rated for a maximum extraction voltage of 5 kV and it is found that above this voltage the reverse electron current in the source is sufficient to cause burning and pitting of the glass baffle. The solenoid magnet current can be adjusted over a range of 0 to 0.6 A. The magnetic flux density, B, at the center of the coil is given by

$$B = \frac{\mu_o NI}{d} \qquad (5.1.1)$$

where N is the number of turns in the coils, d is its average diameter, μ_o is the permeability of air, and I is the electric current. For the magnet used in these experiments, N = 2800 turns and d = 9.21 cm. The peak magnetic field is, therefore, B(Tesla) = 3.82×10^{-2} I(Amperes). From this expression it can be seen that the magnetic field at the center of the magnet is variable from 0 to 0.023 T. In addition, in the experiments described below, three different hydrogen pressures were used, corresponding to throughput values of 0.0012, 0.0042, and 0.0102 Torr liters/sec.

The graphs in Figure 5.1 show the relationship between beam current and probe voltage for different hydrogen throughputs. Each graph was obtained at a magnet current of 0.5 A. It is seen that the beam current rises almost

(a)

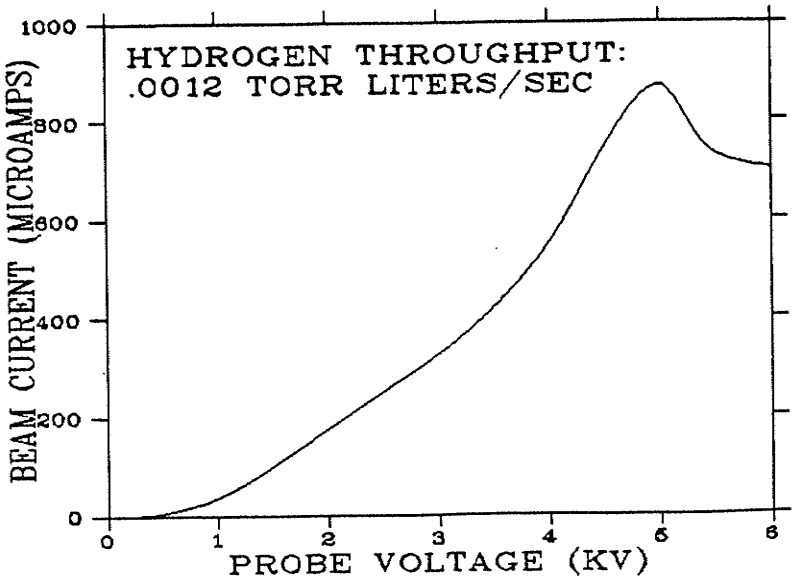

(b)

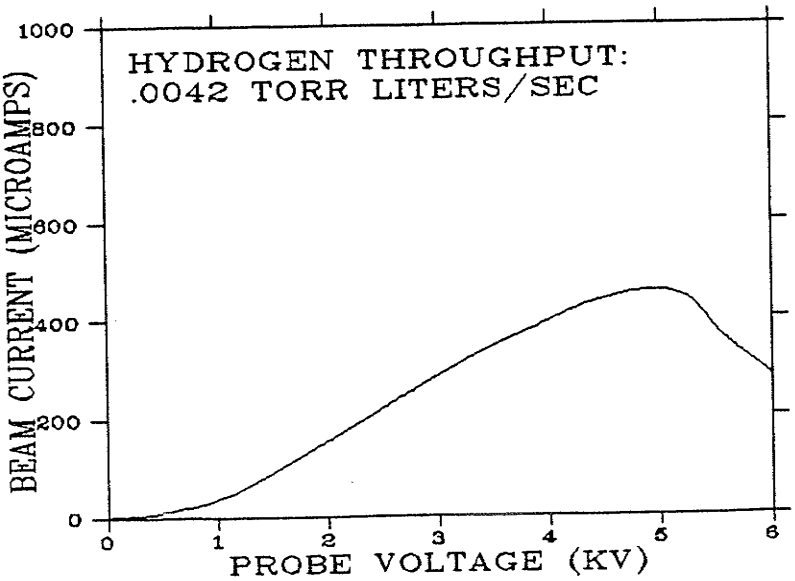

(c)

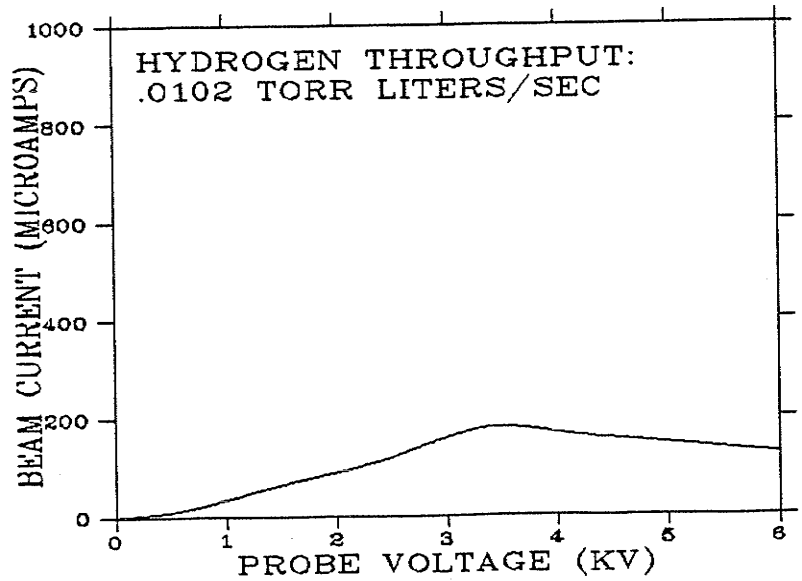

Figure 5.1 Beam Current vs. Probe Voltage

linearly with probe voltage up to a peak value after which it begins to decline. The increase in beam current with probe voltage follows directly from the fact that the current density $J = \sigma E$, where σ is the conductivity of the plasma and E is the applied electric field. The deviation from linearity (particularly evident in Figure 5.1(a)) is due to the fact that σ is not a constant, but is, in part, a function of E.

The drop in current that occurs at around 5.0 kV in Figures 5.1(a) and (b) and at 3.5 kV for (c) is due to saturation of the plasma. At these high extraction fields, ions in the plasma cannot be generated as quickly as they are removed. As the extraction voltage is increased beyond this threshold value, the rate of ion production goes down because electrons are being removed from the plasma before they have a chance to undergo an ionizing collision. The result is a reduction in beam current.

The graphs also show that the beam current decreases with increasing hydrogen throughput. There are two reasons for this effect. First, as the hydrogen pressure is increased beyond the pressure for which $\nu = \omega$ (see section 2.3), the RF power transfer to the plasma is reduced. This is apparent from equation (2.3.10). The extracted beam current which is dependent on the absorbed RF power must, therefore, decrease. Secondly, the increase in recombination that occurs at higher gas pressures contributes to the reduction in ion beam output.

The graphs in Figure 5.2 show the relationship between beam current and magnetic field for different hydrogen flow rates. In general, the presence of a magnetic field serves to increase the beam current. It's effect is most significant at low gas pressures and high probe voltages. The increase in beam current with magnetic field is, as explained in section 2.2, due primarily to increased electron lifetime and a decreased recombination rate.

(a)

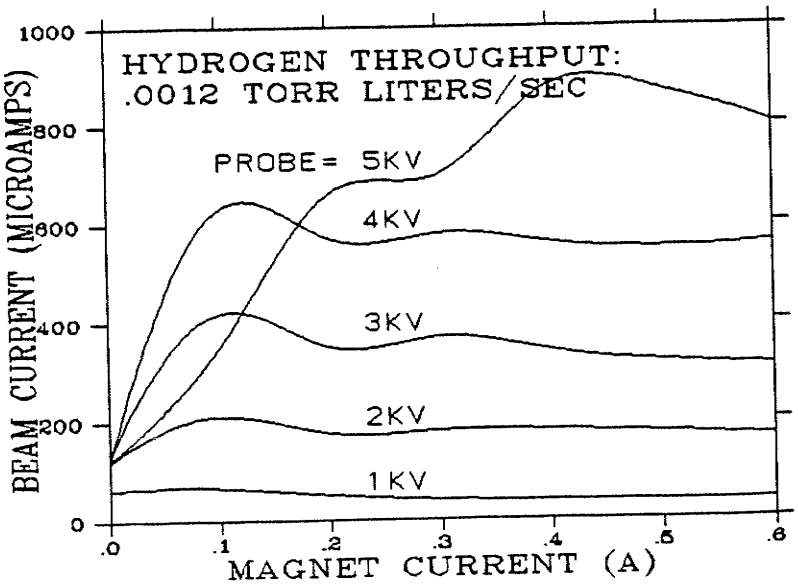

(b)

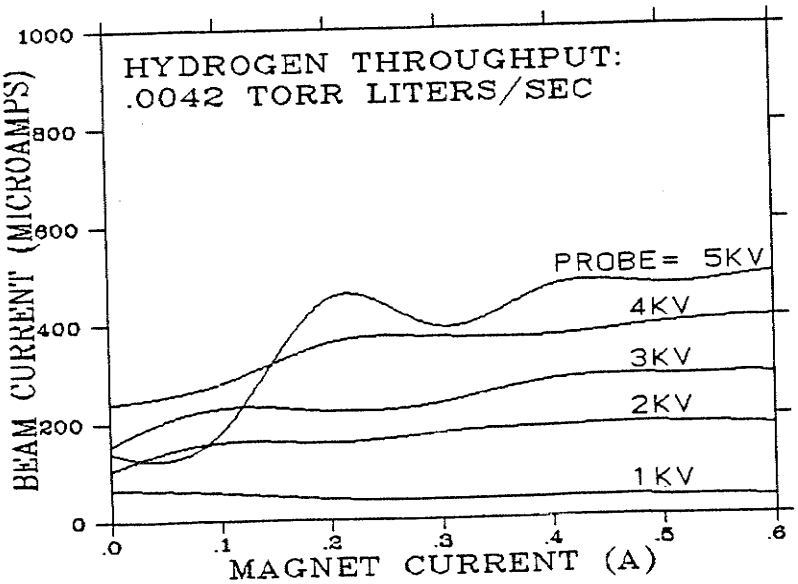

(c)

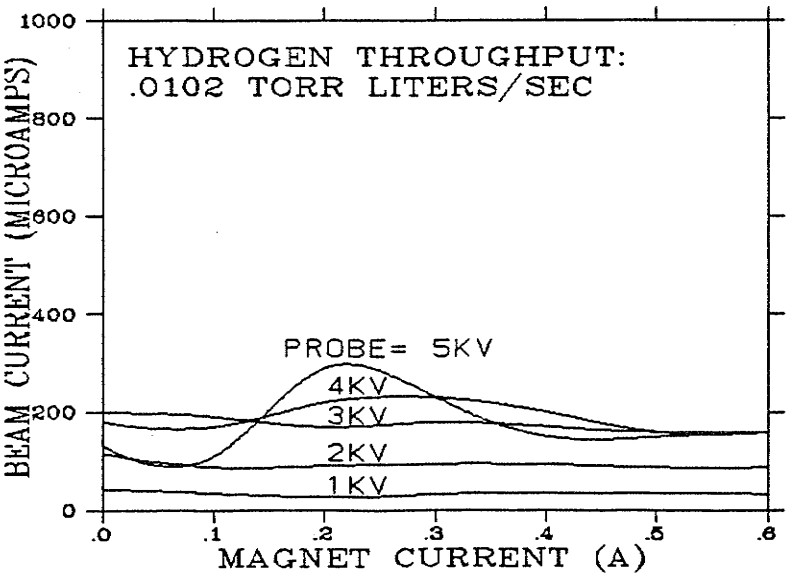

Figure 5.2 Beam Current vs. Magnet Current

It is seen that in almost all cases the beam current curve flattens out as the magnet current is increased beyond around 0.5 A. There is no benefit to be gained by using excessively large magnetic fields. Once the electrons are spiralling tightly about the magnetic flux lines, making them spiral even tighter by increasing the field is not going to have any significant effect on their overall motion or lifetime. In the interest of achieving a low power consumption, the magnet should be operated optimally at the minimum current for which the peak beam current is attained.

It is interesting to note the unusual sort of behaviour exhibited by the 5 kV curve (as well as the 4 kV curve in Figure 5.1(c)) in all three graphs. At these high extraction voltages, the plasma is saturated as is evident from the decreased beam current at zero magnetic field. As the magnetic field is increased, it causes an increase in the electron lifetime and RF power transfer which brings the plasma out of saturation. A dramatic increase in beam current is observed as the source comes out of saturation and back into normal operation.

Particularly apparent in Figure 5.2(a) is the small peak in beam current which occurs at a magnet current of about 0.1 A. This peak may well be due to increased RF power transfer resulting from electron cyclotron resonance. At a magnet current of 0.1 A, the peak magnetic field $B_o = 3.82 \times 10^{-3}$ T and the field whose gyrofrequency (section 6.3) corresponds to the 80 MHz RF frequency is $B_g = 2.86 \times 10^{-3}$ T. At a small distance away from the center of the magnet, it is quite possible that $B_o = B_g$. In such a case, electron heating is increased by electron cyclotron resonance, resulting in an increase in the extracted beam current. If the peaks in Figure 5.2(a) are in fact due to electron cyclotron resonance, then their small amplitude is probably due to the fact that the magnetic field and RF electric field in the C-SO-164 are

nearly parallel. Maximization of the electron cyclotron resonance effect requires that the electric and magnetic fields be orthogonal to one another.

5.2 Ionization Efficiency

The ionization efficiency reflects a source's ability to convert gas molecules into ions. It is simply the ratio of the number of extracted ions to the number of atoms fed into the source. The ionization efficiency is easily calculated, knowing the proton current and the hydrogen throughput.

The throughput of a gas is given by

$$Q = C\Delta P \tag{5.2.1}$$

where C is the conductance of the pumping system and ΔP is the difference in pressure that occurs when a gas flow is introduced. The throughput, normally expressed in Torr liters/sec can be expressed in moles/sec by using the ideal gas law PV = nRT where R is the molar gas constant and T is the absolute temperature. Equation (5.2.1) then becomes

$$Q(\text{moles/sec}) = \frac{C\Delta P}{RT}$$

To obtain the throughput in terms of atoms/sec, the above expression is multiplied by Avagadro's number N_A and also by a factor of 2, since there are two atoms per hydrogen molecule. The throughput, therefore, becomes

$$Q(\text{atoms/sec}) = \frac{2C\Delta PN_A}{RT} \tag{5.2.2}$$

The number of protons leaving the source is simply I/e where I is the proton current and e is the charge of a proton. Assuming that the current extracted from the source is composed entirely of protons, the ionization efficiency η is given by

$$\eta = \frac{IRT}{2eC\Delta PN_A} \tag{5.2.3}$$

It is apparent from equation (5.2.3) that for a given ΔP, the ionization efficiency is proportional to the beam current. The conductance of the VHS-6 diffusion pump with a gate valve and water cooled baffle is listed in the Varian catalog as C = 1200 ℓ/sec. The experiments were conducted at a temperature of T = 300 K. Equation (5.2.3) yields, therefore, $\eta = 7.9 \times 10^{-5}$ I(Amps)/ΔP(Torr).

The background pressure in the vacuum chamber outside the source exit was measured by an ionization gauge as 1.5×10^{-6} Torr. The three different hydrogen flow rates used in these experiments produced gauge pressures of 2.5×10^{-6}, 5×10^{-6}, and 10^{-5} Torr. Knowing that the ionization gauge has a sensitivity of 0.5 for hydrogen, the respective pressure difference are $\Delta P = 2 \times 10^{-6}$, 7×10^{-6}, and 17×10^{-6} Torr. From the pressure differences, it is possible to calculate η from equation (5.2.3) for a given beam current.

The maximum beam current that was obtained in the experiments was I = 930 μA at a pressure difference of $\Delta P = 2 \times 10^{-6}$ Torr. Substituting these values into equation (5.2.3) yields an ionization efficiency of η = 3.7%. This low figure is unfortunately typical of most RF ion sources and, in fact, the figure is somewhat optimistic because it assumes that the extracted beam is made up purely of protons.

5.3 Emittance

All of the emittance measurements were performed with a hydrogen throughput of 0.0042 Torr liters/sec. The probe voltage was varied from 1 to 3 kV and the magnet current was operated over a range of 0 to 0.6 A. The 1 mm wide slit, located 8 cm from the source base was displaced in increments of 1 mm. The scanner was located 82 cm from the slit and the turning radius of the pickup wire was 3.5 cm.

Figure 5.3 shows a typical intensity profile obtained over two scanner revolutions.

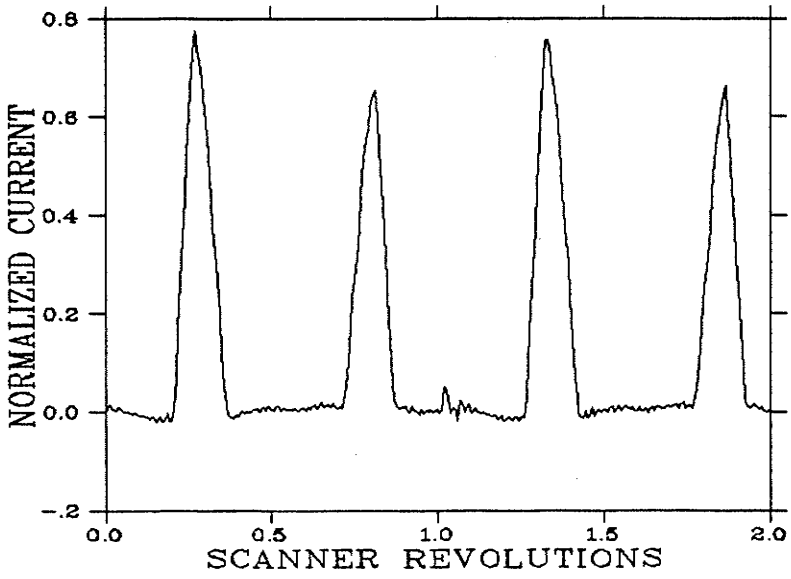

Figure 5.3 Intensity Profile

The current on the y axis is normalized with respect to the peak intensity of the beam. During each revolution of the scanner, two intensity profiles are obtained. The taller peak is obtained when the scanner wire sweeps through the beam during the first half of the revolution, and the smaller one is obtained during the second half of the revolution, when it passes through the beam again. The second peak is smaller in amplitude because it is obtained slightly farther away from the source and so the beam has a chance to diverge more, thereby lowering its intensity. Although the second peak is somewhat smaller in amplitude, it is also slightly wider and integration of the area under each peak shows that they both actually contain the same total current. The small noise glitch occurring at one revolution is caused by a small transient current that is induced in the wire each time the microswitch is triggered.

Figure 5.4 shows the intensity profile of the leftmost peak in Figure 5.3 after the bottom scale has been redefined in terms of divergence angle from equation (4.2.3).

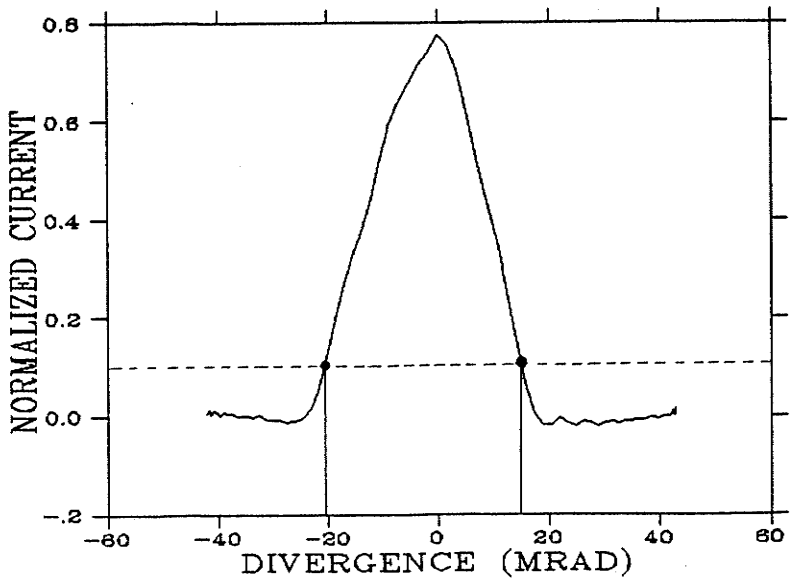

Figure 5.4 Intensity Profile

The dotted line in Figure 5.4 depicts the level for which the current is 10% of the peak current intensity. From this level, the divergence angles are picked off of the bottom axis in order to obtain two points for a 10% brightness contour.

Figure 5.5 shows a number of brightness contours obtained for the C-SO-164 in the vertical plane with a probe voltage of 2 kV and a magnet current of 0.2 A.

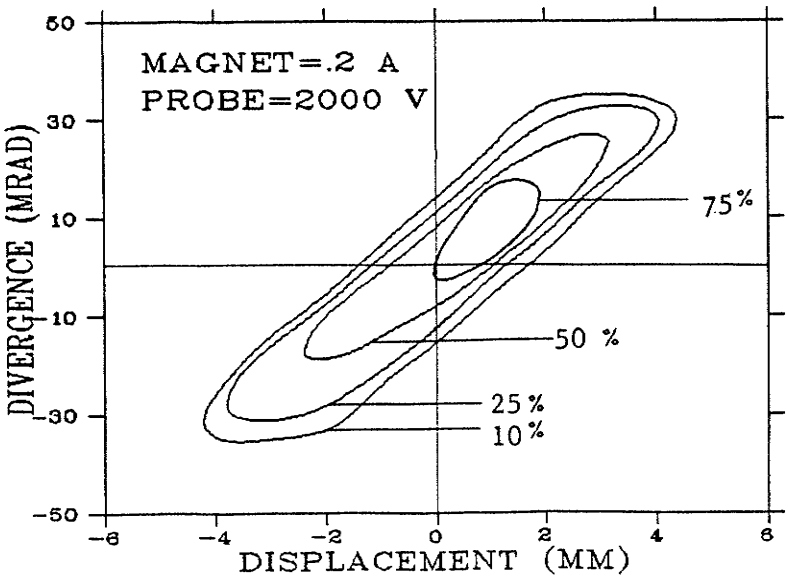

Figure 5.5 Brightness Contours

The different contours help to show the intensity distribution of the beam. It is apparent that in the vertical plane, the region of highest intensity lies a small distance off the central axis.

The 10% brightness contours in both the horizontal and vertical planes were measured and plotted over the range of probe voltage and magnet current. The contour plots are all shown in Appendix B. The phase space area within each contour plot was also measured and the results are tabulated in Tables 5.1 and 5.2.

Table 5.1 Vertical Emittance (mm mrad)

	Probe Voltage		
Magnet Current	1000 V	2000 V	3000 V
0 A	257.2	186.8	180.6
0.2 A	248.8	186.2	181.0
0.4 A	244.5	220.5	205.3
0.6 A	241.5	220.0	213.5

Table 5.2 Horizontal Emittance (mm mrad)

	Probe Voltage		
Magnet Current	1000 V	2000 V	3000 V
0 A	243.5	189.8	173.5
0.2 A	251.3	198.3	186.5
0.4 A	253.0	210.0	199.5
0.6 A	250.8	219.8	205.5

The results of tables 5.1 and 5.2 are summarized by the graphs in Figure 5.6(a) and (b).

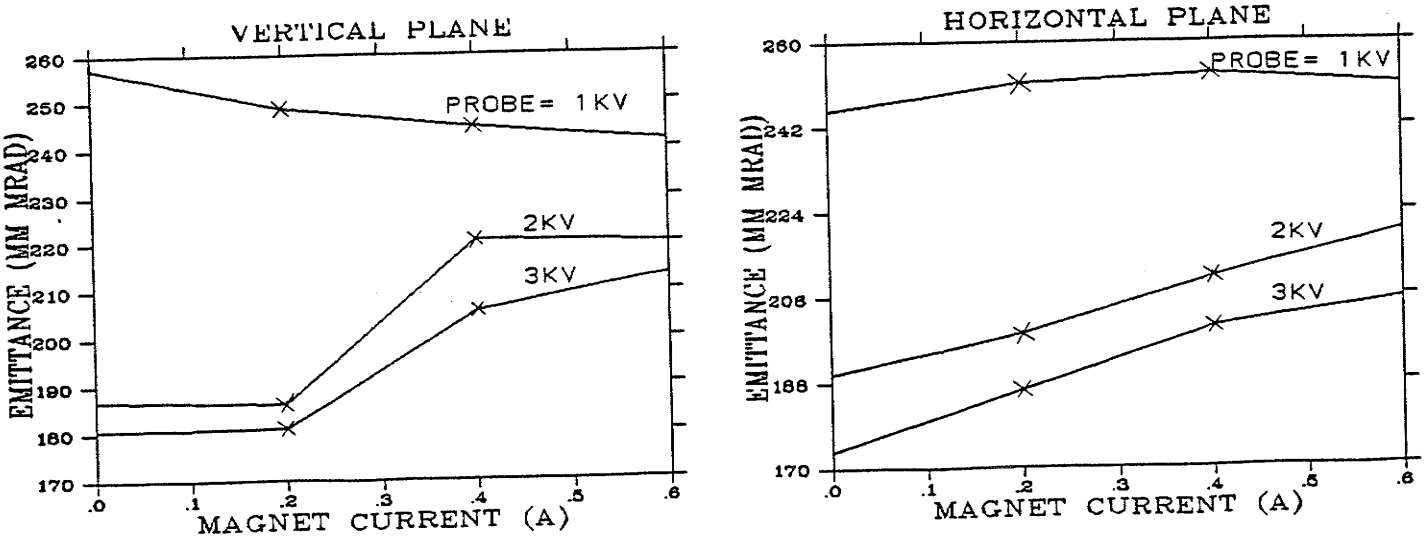

(a) (b)

Figure 5.6 Emittance Characteristics

The graphs seem to indicate that similar trends exist in both the horizontal and vertical planes. It is seen that the emittance decreases with increasing probe voltage and that the amount by which it decreases gets smaller with increasing voltage. This result is not surprising since, neglecting space charge, the emittance is inversely proportional to the square root of the ion energy. In this case, because increasing the probe voltage also increases the

beam current, and hence the space charge, the proportionality does not quite hold. This becomes even more evident at higher magnet currents as seen in Figure 5.6(a) and (b).

At probe voltages of 2 and 3 kV, the emittance increases with magnetic field, displaying a slight leveling off at 0.4 to 0.6 A. From Figure 5.2(b), it is seen that at these probe voltages the beam current tends to increase with magnet current. This increase in beam current produces an increase in space charge which is reflected by an increase in emittance. In the case of the 1 kV probe voltage, there is little change in emittance with magnet current. In fact, in Figure 5.6(a) the vertical emittance actually decreases slightly. The reason for this becomes apparent from Figure 5.2(b). At a 1 kV probe voltage, the magnetic field has only a very slight decreasing effect on the beam current. Since there is little change in beam current at this voltage, there will likewise be little effect on the emittance due to the magnetic field.

It is quite obvious that space charge plays a significant role in beam optics at the high currents and low energies that are typically attained with the C-SO-164. It is an unfortunate fact that anything which contributes to producing a higher beam current for a given ion energy, will result in a larger emittance due to the effects of space charge.

CHAPTER VI

MICROWAVE AND ECR ION SOURCES

6.1 History

In the 1960s microwave discharges were used as excitation sources for gaseous electronics studies, for light sources, and for production of free radicals. More recently, microwave sources have found use in neutral beam heating for fusion research as well as various other applications.

Richard Geller was the first person to employ electron cyclotron resonance (ECR) in a microwave source and he has been largely responsible for the development of ECR sources up to the present. His first ECR source [17], developed in the mid 1960s, was designed for high current operation and was able to produce beam currents of 20 mA with a microwave power of 250 W at 10 GHz.

In the early 1970s Geller developed MAFIOS (Machine For Ion Stripping) [18,19], an ECR source intended for the production of multiply charged ions. MAFIOS consisted of a quartz discharge tube passing through a resonant cavity. A solenoid produced, magnetic-bottle field was superimposed on the discharge tube. Consuming 500 W of microwave power at 10 GHz, MAFIOS was able to produce a nitrogen beam of 23 mA in various charge states.

The first true high performance ECR ion source was called SUPERMAFIOS [19,20]. Also built by Geller, SUPERMAFIOS was the first ECR source to employ a hexapole magnetic field for plasma confinement. SUPERMAFIOS was a two-stage device, permitting plasma to be created in a high pressure region, but heated and accumulated in a low pressure region. Operated from 1974 to 1977,

SUPERMAFIOS consumed 3 MW of power (1 kW of microwave power) and was able to produce xenon ions with a charge as high as 19.

In 1979 Geller built a scaled-down version of SUPERMAFIOS called MICROMAFIOS [21]. By utilizing $SmCo_5$ permanent magnets, in place of the electromagnets, he was able to produce a much more compact source, consuming only 100 kW of power (2 kW of microwave power).

At the same time that Geller was developing MICROMAFIOS, Jongen and Ryckewaert [22] were working on ECREVIS. ECREVIS was similar in concept to SUPERMAFIOS except that it used superconducting magnets in order to reduce the power consumption. ECREVIS consumed a total power of 100 kW. 200 W of microwave power were absorbed in the injector stage, at 8.5 GHz, while the main stage used 2.5 kW of power at 14.3 GHz. A smaller version of ECREVIS, called ECREVETTE [22], was built in the early 1980s.

In Japan, ECR was being exploited to develop extremely compact high current sources. In 1979, Sakamoto [23] developed a source from which he was able to extract 40 mA of protons. The source consumed 250 W of microwave power at 4.4 GHz. The power is transmitted into the discharge by means of a small antenna. Because of the small dimensions of the source, the discharge chamber does not form a resonant cavity. The entire source body is constructed of ferromagnetic material and, in fact, it forms a magnetic circuit which concentrates the magnetic field in the discharge region. A similar source was constructed in 1983 by Ishikawa et al. [24] for the high current production of Cs and Rb metal ions.

There are still many new ideas and advances occurring in ECR ion source technology and the present trend indicates that many large accelerator facilities are turning to ECR sources as a means for producing highly charged ion beams.

6.2 Microwaves as a Means for Plasma Production

Electron heating through microwave excitation has proved to be one of the most efficient methods for producing a plasma from which an ion beam can be extracted. The microwave discharge produces a high degree of ionization and a large amount of molecular dissociation without undue heating of the background gas. With no need for internal electrodes, it is possible to construct reaction vessels which are simple, rugged, and free from contamination.

At microwave frequencies, it becomes practical to use waveguides to transport the high frequency energy. Since there is no radiation from waveguides and very little dielectric loss, attenuation of the transmitted power is very small. Also, by placing the discharge inside a resonant cavity it is possible to greatly increase the electric field in the discharge through constructive interference. When microwaves are fed into a resonator, the microwave field will build up until the energy flow into the cavity is balanced by the outgoing energy flow plus the internal damping. Because the losses in the cavity wall are small, the damping is almost entirely due to electron heating. Ion heating is negligible compared to the electron heating due to the greater masses of the ions. The power absorbed by the plasma can be measured as the difference between the power entering and leaving the resonator.

Although there exist a wide variety of ion sources, which employ microwaves as a means for plasma generation, they can be classified generally into two categories. The first type is the most simple; consisting of a glass or quartz discharge tube contained partly or entirely within a resonant cavity. Power is usually fed to the cavity by coaxial cable and emitted either by a small coupling loop or a probe antenna. This type of source is

usually intended for high-current, low-charge state applications and may, or may not, employ a static magnetic field for electron cyclotron resonance.

In the second class of sources, the walls of the discharge chamber form a multimode cavity. Because the inside of the cavity is maintained at a low gas pressure, the microwave power is delivered from a waveguide into the discharge chamber, through a vacuum sealed teflon or quartz window. A multicusp magnetic field is used to confine the plasma and an axial magnetic-bottle field is produced by solenoid magnets to induce electron cyclotron resonance. These ECR sources tend to be large and complex, often consisting of several stages. They are used primarily in applications requiring low currents and high charge states.

6.3 The Microwave Discharge

There are certain plasma characteristics which tend to take on a significant role at the high frequencies and plasma densities that are typically attained in the operation of microwave ion sources. Electron cyclotron resonance, for instance, can be used to enhance the power transfer to the plasma, while too dense a plasma can cause a reduction in power transfer. Such factors ultimately determine the intensity and quality of the extracted ion beam.

6.3.1 Plasma Oscillations

Neglecting all loss mechanisms in a neutral plasma under the influence of no electric field, it is found that the electrons have a natural frequency of oscillation called the "plasma frequency" [25]. Consider a neutral plasma in an undisturbed equilibrium state. The positive ions can be considered stationary because of their large mass. Suppose now that some electrons are

disturbed from their equilibrium state. Because the electron density in one region is increased, the electrons will tend to repel each other back toward their equilibrium positions. Instead of coming to rest in their equilibrium positions, they overshoot. The result is an oscillation about the equilibrium position.

The equation of motion for an electron in a plasma was given in equation (2.3.6) as

$$m_e \frac{d\underset{\sim}{v}_e}{dt} + m_e \nu \underset{\sim}{v}_e = e\underset{\sim}{E}$$

Assuming no external electric field and a time dependent velocity of $\exp(j\omega t)$, the equation of motion becomes

$$j\omega m_e \underset{\sim}{v}_e + m_e \nu \underset{\sim}{v}_e = -e\underset{\sim}{E} \tag{6.3.1}$$

In this case the electric field E results from the electron's displacement from its equilibrium position. The average current density at any instant due to the motion of the electrons is given by

$$\underset{\sim}{J} = - n_e e \underset{\sim}{v}_e \tag{6.3.2}$$

and, therefore, the average electron velocity is

$$\underset{\sim}{v}_e = - \frac{\underset{\sim}{J}}{en_e} \tag{6.3.3}$$

Substituting equation (6.3.2) into (6.3.1) yields

$$\underset{\sim}{J} = \frac{n_e e^2}{j\omega m_e} \underset{\sim}{E} \tag{6.3.4}$$

Maxwell's fourth equation states that

$$\nabla x \underset{\sim}{H} = \underset{\sim}{J} + \frac{\partial \underset{\sim}{D}}{\partial t}$$

where $\partial \underset{\sim}{D}/\partial t$ is the displacement current density. Since in this case there is no magnetic field ($\nabla x \underset{\sim}{H} = 0$), the electron current density and displacement current density can be equated as

$$\underset{\sim}{J} = - j\omega\varepsilon_o \underset{\sim}{E} \tag{6.3.5}$$

Assuming no collisions ($\nu = 0$), equating (6.3.4) with (6.3.5) produces the following result:

$$\omega^2 = \frac{n_e e^2}{m_e E_o}$$

The frequency of electron oscillation or plasma frequency is therefore

$$\omega_p = \left[\frac{n_e e^2}{m_e E_o}\right]^{1/2} \tag{6.3.6}$$

6.3.2 Wave Attenuation

The plasma behaves as a conducting medium with a conductivity that is a function of frequency. This means that the permittivity of the plasma will be in the form of a complex number. In a medium of finite conductivity, the current density is given by

$$\underset{\sim}{J} = \sigma \underset{\sim}{E}$$

Substituting this current density into Maxwell's fourth equation

$$\nabla \times \underset{\sim}{H} = \sigma \underset{\sim}{E} + j\omega\varepsilon \underset{\sim}{E} = j\omega(\varepsilon - j\frac{\sigma}{\omega})\underset{\sim}{E} \tag{6.3.7}$$

From equation (6.3.7) we define an effective permittivity of

$$\varepsilon_{eff} = \varepsilon - j\frac{\sigma}{\omega} \tag{6.3.8}$$

We can rewrite the current density (equation (6.3.2)) in terms of the plasma frequency (equation (6.3.6)). The resulting expression is

$$J = \frac{\varepsilon_o \omega_p^2}{\omega^2 + \nu^2}(\nu - j\omega) \tag{6.3.9}$$

From equation (6.3.7) it is seen that

$$j\omega\varepsilon_{eff} E = J + j\omega\varepsilon_o E \tag{6.3.10}$$

Substituting equation (6.3.4) into equation (6.3.10) and comparing the result with equation (6.3.9) it is apparent that the effective permittivity is given by

$$\varepsilon_{eff} = \underbrace{\varepsilon_o\left[1 - \frac{\omega_p^2}{\omega^2 + \nu^2}\right]}_{\varepsilon} - j\underbrace{\frac{\varepsilon_o \nu \omega_p^2}{\omega(\omega^2 + \nu^2)}}_{\sigma/\omega} \tag{6.3.11}$$

The complete expression for the electric field of a plane wave travelling in the forward z direction is given by

$$E = E_o \exp(j\omega t - \gamma z)$$

where γ is known as the "propagation constant". the propagation constant consists of a real and an imaginary component.

$$\gamma = \alpha + j\beta$$

β is called the "phase constant" and it determines the position of the wave at a given instant of time. α is the "attenuation constant" and if it is non-zero the wave decays exponentially with distance. For the effective permittivity given in equation (6.3.8), the square of the propagation constant is

$$\gamma^2 = -\omega^2\mu\left(\varepsilon - j\frac{\sigma}{\omega}\right) \tag{6.3.12}$$

where μ is the permeability of medium through which the wave propagates ($\mu = \mu_o$ for a plasma). Substituting ε and σ from equation (6.3.11) into equation (6.3.12) yields

$$\gamma^2 = -\omega^2\mu_o\varepsilon_o\left[\left(1 - \frac{\omega_p^2}{\omega^2 + \nu^2}\right) - j\frac{\nu\omega_p^2}{\omega(\omega^2 + \nu^2)}\right] \tag{6.3.13}$$

From equation (6.3.13) it can be shown that the attenuation constant α is given by the expression,

$$\alpha = \sqrt{\frac{1}{2}\omega^2\mu_o\varepsilon_o\left[1 - \frac{\omega_p^2}{\omega^2 + \nu^2}\right]\left\{-1 - \sqrt{1 + \left(\frac{\nu\omega_p^2}{\omega(\omega + \nu^2 - \omega_p^2)}\right)^2}\right\}} \qquad (6.3.14)$$

From equation (6.3.14) it is apparent that in order for α to be positive and real,

$$\omega^2 < \omega_p^2 - \nu^2$$

Under such conditions a plane wave will be attenuated as it propagates through the plasma. Essentially the plasma has the characteristics of a high pass filter with a cut-off frequency of $\sqrt{\omega_p^2 - \nu^2}$. It is evident that an increase in the collision frequency lowers the cut-off frequency and decreases the attenuation constant thereby increasing penetration of the wave into the plasma. This effect is due to the decrease in the electrical conductivity of the plasma that occurs with increasing collision frequency.

It is usually assumed that $\nu << \omega$ in which case the cut-off frequency of the plasma is simply the plasma frequency. The density of the plasma is ultimately limited by the cut-off density for wave propagation. From equation (6.3.5) it is easily seen that this cut-off density is given by

$$n_{cut\text{-}off} = \frac{\omega_p^2 m_e \varepsilon_o}{e^2} \qquad (6.3.15)$$

For efficient operation of a microwave ion source, the designer must ensure that the plasma will not get so dense as to result in power loss through plasma conductivity.

6.3.3 Electron Cyclotron Resonance

In a magnetically biased lossless ($\nu = 0$) plasma, the equation of motion for an electron is

$$m_e \frac{dv_e}{dt} = e(E + v_e \times B) \qquad (6.3.16)$$

where B is the magnetic flux density. If the magnetic field is homogeneous in the z direction and the plane wave is propagating along the x-z plane, then equation (6.3.16) can be written in scalar component form as

$$\frac{m_e}{e}\frac{dv_x}{dt} = E_x + v_y B_z \tag{6.3.17a}$$

$$\frac{m_e}{e}\frac{dv_y}{dt} = E_y + v_x B_z \tag{6.3.17b}$$

$$\frac{m_e}{e}\frac{dv_z}{dt} = E_z \tag{6.3.17c}$$

Assuming harmonic motion of the wave and charged particle, solution of its component velocities are as shown below.

$$v_x = \frac{j(m_e\omega/e)E_x + B_z E_y}{B_z^2 - (m_e\omega/e)^2} \tag{6.3.18a}$$

$$v_y = \frac{j(m_e\omega/e)E_y + B_z E_x}{B_z^2 - (m_e\omega/e)^2} \tag{6.3.18b}$$

$$v_z = -\frac{j_e E_z}{m_e\omega} \tag{6.3.18c}$$

From the relations (6.3.18) it can be inferred that the wave will cause the electron to move along a helical path with axis coincident with the magnetic field (z direction). The implication of this is that the magnetic field can be used as a tool for confining and concentrating the plasma, since the electrons and ions will tend to spiral along the magnetic flux lines. Furthermore, it can be seen that v_x and v_y become infinite when the wave frequency is

$$\omega = \frac{e}{m_e} B_z \tag{6.3.19}$$

This condition is known as "electron cyclotron resonance" and it occurs when the electron's "gyrofrequency", that is the frequency at which it revolves in

a magnetic field, coincides with the excitation frequency. In a lossy plasma the velocities would never in fact become infinite because the resistance due to collision eventually balances the accelerating force and the electron attains an equilibrium velocity.

6.4 ECR for High Current Ion Production

It has been shown that microwave discharges in a magnetic field are capable of producing plasma with a large number of high energy electrons [26]. If such a high energy electron undergoes an ionizing collision, it still has enough energy to cause further ionization, whereas in a plasma with low temperature electrons this is not the case. In non-resonance electron heating, the electrons are accelerated for one half-cycle of each microwave oscillation and then decelerated for the next half-cycle. Whatever energy the electron has not expended by collisions during the acceleration half-cycle is returned to the field in the deceleration half-cycle.

When there is electron cyclotron resonance, however, the electron gains energy with each oscillation and will continue to accelerate until the power dissipation due to collisions equals the microwave power or until the electron strikes the walls of the reaction vessel. Because of this energy storage phenomenon, electron cyclotron resonance has proved to be very efficient for transferring power to a plasma. Lichtenberg and Liebermann [27] have found that for a hydrogen plasma, the electron temperatures tend rapidly to an upper limit given roughly by

$$T_{e(keV)} = P_{RF(W)}^{3/8} \qquad (6.4.1)$$

where $P_{RF(W)}$ is the high frequency power in watts. From the above expression it can be seen that the electron temperatures in the keV range can be reached with as little as 100 W of microwave power.

The ion current density that can be extracted from a plasma is approximated by the following expression

$$J \simeq n_i e(kT_e/M)^{1/2} \qquad (6.4.2)$$

where k is Boltzman's constant, n_i is the ion density, T_e is the electron temperature and M is the ion mass. It is evident from equation (6.4.2) that a high current ion source should have a plasma with a high ion density and a high electron temperature. At the same time, the ion temperature should be low enough to obtain an ion beam with a low energy spread and low emittance. When the plasma electrons are selectively heated by means of the ECR process, only the electron temperature can be increased while the ion temperature is kept low. Therefore, the ECR process is quite suitable for the production of high density singly-charged ions [24]. In this case, the divergence angle of the ion beam, which is proportional to the square root of the ion temperature, will be small. This means that the emittance of an ion beam produced by ECR will be low.

CHAPTER VII

MODIFYING THE C-SO-164

7.1 General Design Considerations

The modification of the C-SO-164 consists essentially of the replacement of the RF excitation system with microwave excitation. The source will still operate in the same manner as before, and so, no changes need to be made to the source bottle, base flange or extraction system. As an RF ion source, the 80 MHz RF power was coupled into the C-SO-164 by means of two ring electrodes. In the microwave version, the power will be fed into the source bottle through a short section of waveguide acting as a resonator at 2.45 GHz. The primary advantages of the microwave version are a higher beam current due to the increased density of the microwave plasma, and the reduced power consumption attributable to the low loss nature of the waveguide.

7.1.1 The Resonator

Figure 7.1 shows the general layout of the microwave source. The closed-off ends of the waveguide cause it to behave as a resonant cavity. The cross-sectional dimensions of the inside of the cavity conform to the specifications of a WR-340 waveguide designed to transmit a TE_{10} mode wave over a frequency range of 2.20 to 3.30 GHz. In this frequency range, only the fundamental mode of oscillation can be sustained by the waveguide, since all other modes occur at frequencies below the cut-off frequency.

The length of the cavity is one waveguide wavelength. The wavelength of a wave propagating through a rectangular waveguide is somewhat longer than

that of a plane wave of identical frequency travelling through an unbounded medium. For an air-filled, rectangular waveguide, the waveguide wavelength is given by

$$\lambda_g = \frac{\lambda_o}{\sqrt{1 - \left(\frac{\lambda_o}{\lambda_c}\right)^2}} \tag{7.1.1}$$

where λ_o is the wavelength of a plane wave in air and λ_c is the cut-off wavelength of the waveguide. The cut-off wavelength is described by the expression,

$$\lambda_c = \left[\left(\frac{m}{2a}\right)^2 + \left(\frac{n}{2b}\right)^2\right]^{-1/2} \tag{7.1.2}$$

where m and n are the mode numbers (1 and 0, respectively for the TE_{10} mode), and a and b are the cross-sectional dimensions of the waveguide. For a WR-340 waveguide, the dimensions are a = 8.64 cm and b = 4.32 cm. From equation (7.1.2), therefore, the cut-off wavelength is λ_c = 17.28 cm. The wavelength λ_o is simply obtained from $\lambda_o = c/f$ = 12.24 cm, where c is the speed of light in air and f is the frequency. Substituting the values for λ_c and λ_o into equation (7.1.1), it is found that the waveguide wavelength is λ_g = 17.35 cm. The cavity will be resonant, if its overall length is an integral number of half-wavelengths. The source bottle and the magnetron output are each located one-quarter wavelength from the ends of the cavity, in the regions of peak electric field.

The presence of a discharge changes the resonant frequency and the loaded Q-factor of the resonator [28]. Furthermore, the properties of the discharge change with pressure and electric field. Changes in operating conditions of the source can result in a loss of resonance which leads to a reduction in the power absorbed by the discharge. In order to keep the cavity

in resonance, a tuning plunger is used to adjust the length of the cavity (Figure 7.1).

The cylindrical sleeves surrounding the source bottle on both sides of the waveguide prevent microwave power from radiating. The sleeves themselves form cylindrical waveguides in which there is no propagation, because the 2.45 GHz microwave frequency is well below the sleeves' cut-off frequency. The inner diameter of the sleeves is made slightly larger than the diameter of the source bottle to permit cooling air to circulate through the cavity and over the surface of the bottle.

The resonator will be fabricated from 1/32" aluminum sheets. Aluminum was chosen because of its good electrical conductivity, low cost, and ease of fabrication. Appendix C shows a detailed 3-view illustration of the resonator. At the time of writing, some of the aluminum sheets have already been cut, polished, and drilled.

7.1.2 The Solenoid Magnet

The solenoid magnet serves two primary functions. First of all, it increases electron lifetime and concentrates the plasma in the region near the exit hole, as described in section 2.2. Secondly, if the magnetic field is of the correct strength, it induces electron cyclotron resonance, thereby increasing the efficiency of power transfer to the plasma. The magnetic flux density required to produce electron cyclotron resonance at 2.45 GHz is obtained from equation (6.3.19) as $B_{ECR} = .0785$ T. Figure 7.2 illustrates the electric and magnetic fields inside the source bottle. The ECR heating will be most effective in the regions in which the mutually orthogonal components of the electric and magnetic field are the greatest.

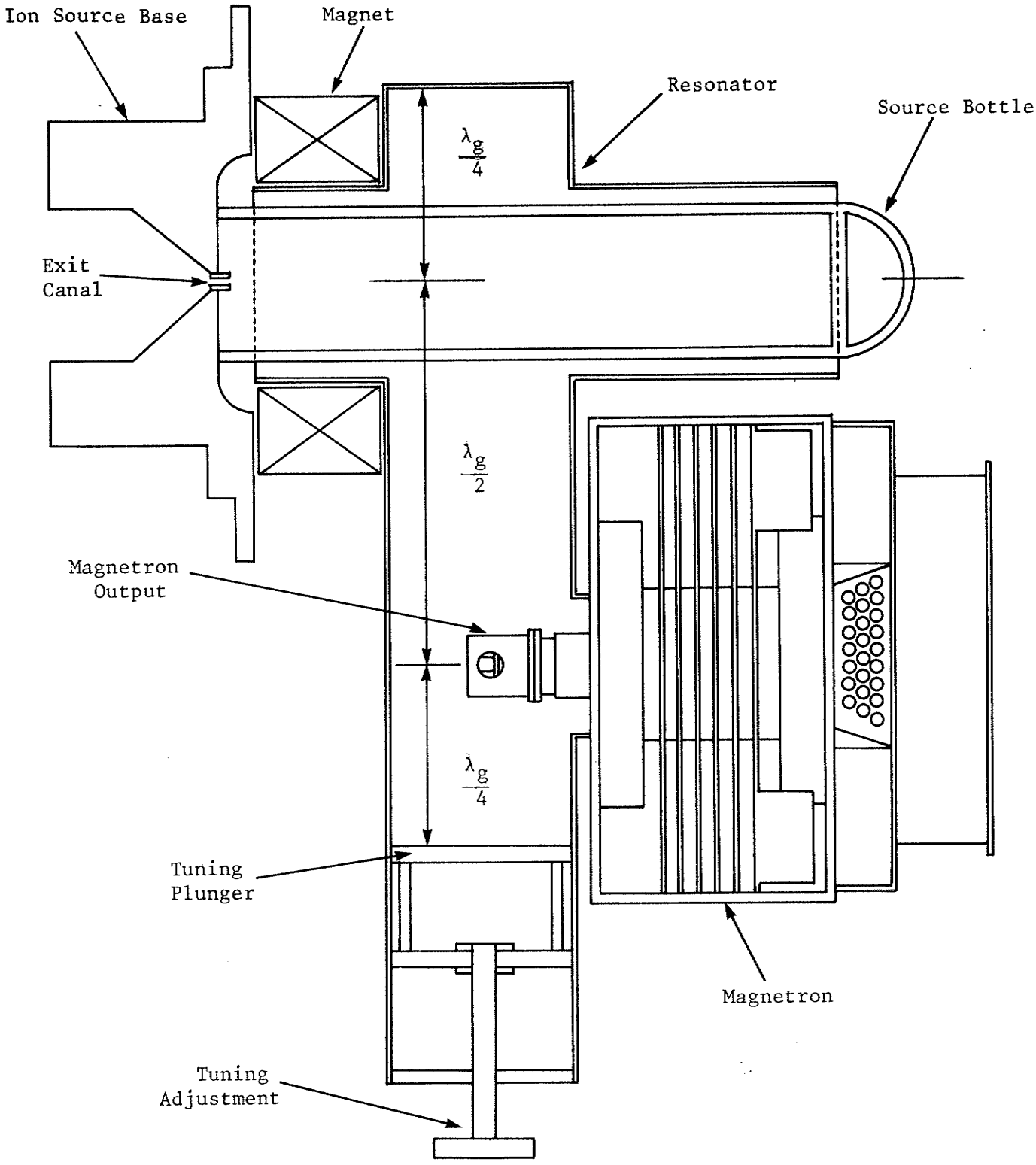

Figure 7.1 The Resonator

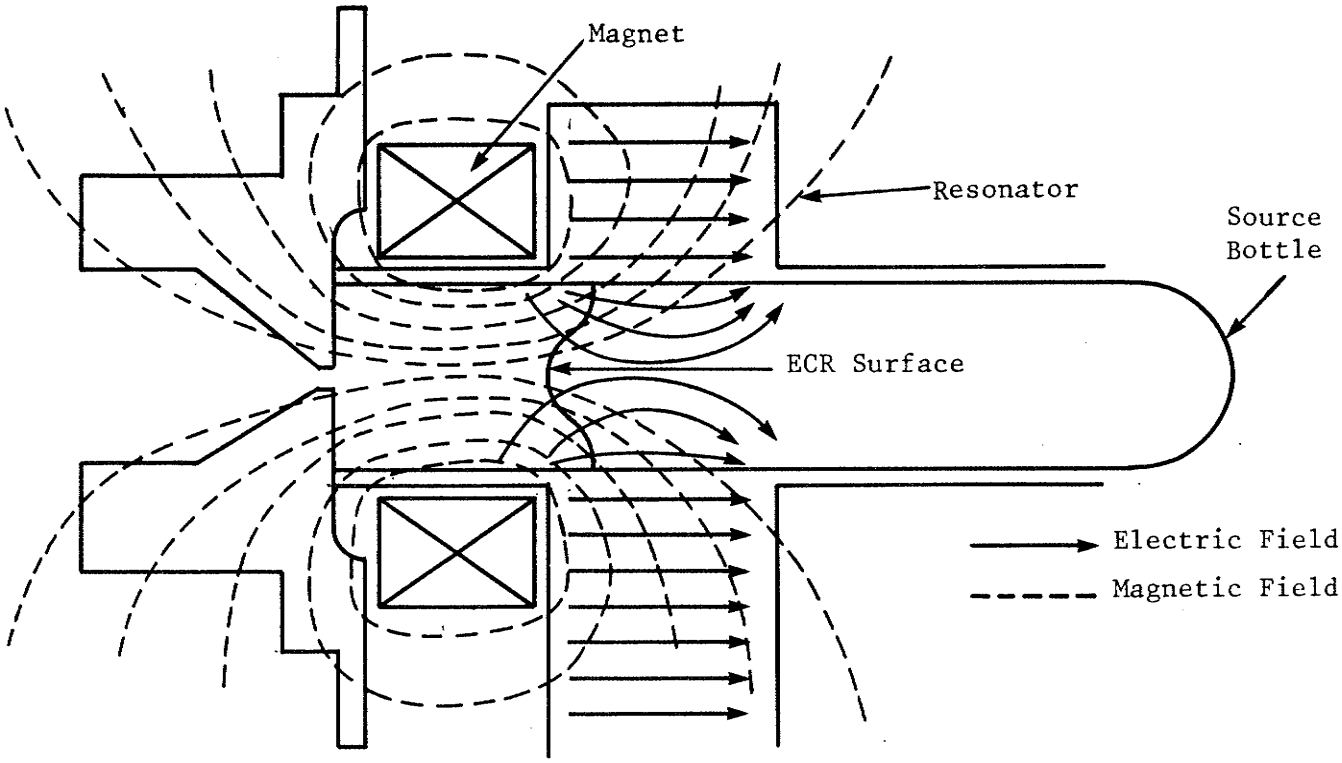

Figure 7.2 Electric and Magnetic Fields in the Source Bottle

The ECR region is represented by a surface of constant magnetic flux density ($B = B_{ECR}$).

To ensure that the magnetic field strength will be sufficient to induce ECR inside the resonator, the flux density at the center of the magnet should be at least $1.5 \times B_{ECR}$. For a frequency of 2.45 GHz, this corresponds to a flux density of roughly B = .12 T. A field of this magnitude is very close to the upper limit of what can be attained practically from an air-cooled solenoid. The coil, therefore, must be carefully designed to minimize the power consumption.

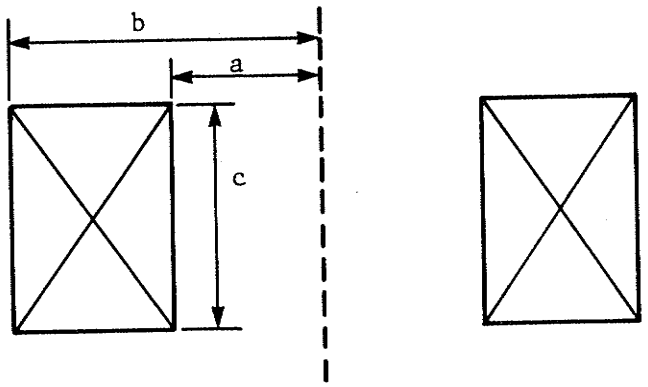

Figure 7.3 The Solenoid Magnet

For the coil shown in Figure 7.3, the a and c dimensions are fixed at 2 cm and 3 cm, respectively, so that the magnet can fit between the waveguide and the ion source base. For #22 gauge wire, the packing density, D, is about 230 cm^{-2} and the resistance per unit length is $R_o = .075\Omega/m$. The two variable parameters are the magnet current I and the outer magnet radius b (which determines the number of turns N).

From equation (5.1.1) the magnetic flux density at the center of the coil is

$$B_o = \frac{\mu_o NI}{d}$$

From Figure 7.3, the average coil diameter is d = a+b. The number of turns in the coil is given by

$$N = c(b - a)D \tag{7.1.3}$$

Substituting the expressions for d and N into equation (5.1.1) yields

$$B_o b - \mu_o cDIb + \mu_o cDaI = -B_o a \tag{7.1.4}$$

It can be seen that equation (7.1.4) is an expression of the form

$$Ab + BbI + CI = D \tag{7.1.5}$$

where

$$A = B_o \tag{7.1.6a}$$

$$B = -\mu_o cD \tag{7.1.6b}$$

$$c = -aB \tag{7.1.6c}$$

and

$$D = -aA \tag{7.1.6d}$$

From equation (7.1.5)

$$b = \frac{(D - CI)}{(A + BI)}$$

and by substituting equations (7.1.6c) and (7.1.6d) into the above equation,

$$b = \frac{(BI - A)}{(A + BI)} a \tag{7.1.7}$$

Now the power dissipated as heat within the coil is

$$P = I^2R = I^2\pi R_o(b^2 - a^2)Dc \tag{7.1.8}$$

Substituting equation (7.1.7) into (7.1.8) produces the following expression for power.

$$P = I^2\pi R_o a^2 D\left[\left(\frac{BI - A}{A + BI}\right)^2 - 1\right] \tag{7.1.9}$$

In order to find the optimum current for minimum power, equation (7.1.9) is differentiated with respect to I and equated to zero. After some simplification, the result is

$$\frac{\partial P}{\partial I} = 0 = (A+BI)(BI-A)(2BI-A) - I(BI-A)^2B - (A+BI)^3 \tag{7.1.10}$$

The solutions to the above cubic equation are I = 0, ∞, -3A/B. The I = 0 and I = ∞ solutions can be disregarded because they represent magnets with infinite and zero number of turns, respectively. The maximum current to the coil is therefore,

$$I = -\frac{3A}{B} = \frac{3B_o}{\mu_o cD} \tag{7.1.11}$$

This corresponds to a current of 4.15 A. Substituting this result into equation (7.1.7) shows that the outer radius b = 2a = 4 cm. From equation (7.1.3) the number of turns can be calculated as 1380 and from equation

(7.1.8) it is seen that the maximum power dissipation is 336 W. Table 7.1 summarizes the specifications of the magnet.

Table 7.1 Magnet Specifications

dimensions	a : 2 cm
	b : 4 cm
	c : 3 cm
resistance	19.5 Ω
turns	1380
max. current	4.15 A
max. B at center	.12 T
max. power dissipation	336 W

The 336 W power dissipation is quite excessive for an air-cooled solenoid and it probably would not be practical to operate the magnet at full power for more than several minutes at a time. However, once experiments have established the optimum magnet current for maximum power transfer to the plasma (see section 7.4), the solenoid should be replaced with a permanent magnet having similar field characteristics.

7.1.3 The Magnetron

The microwave power for the source is supplied by a Sanyo 2M57-A microwave oven magnetron. The magnetron is rated at a power output of 600 W, at an anode voltage of -4 kV. It was chosen to mount the magnetron directly onto the resonator for simplicity and for most efficient power coupling. This direct coupling method does not permit impedance matching so that the magnetron will be entirely exposed to the reflected power. In most microwave systems, circulators are used to redirect any reflected power into a dummy load, in order to protect the microwave generator. In this case, however,

because microwave oven magnetrons are sturdily built to withstand considerable reflected power, and because the magnetron will be operating at a small fraction of its rated power, there should be little risk of damage.

The basic structure of the magnetron is shown in Figure 7.4. A resonant cavity is formed by a number of vanes made of heat conductive copper. An electron emitting cathode is positioned along the central axis of the cylinder. In addition, two permanent magnets are used to produce an axial magnet field in the interaction space between the vanes and the cathode. A small probe antenna in one of the cavities directs the microwave power to the output.

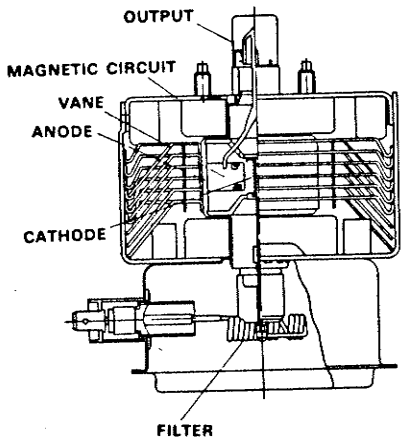

Figure 7.4 The Magnetron

A negative high voltage applied to the cathode creates a static electric field between the vanes and the cathode. Electrons emitted by the cathode move toward the anode along spiral paths under the combined influence of the electric and magnetic fields. The spiral movements of electrons are bunched together by the high frequency electric field generated in the resonator by induction.

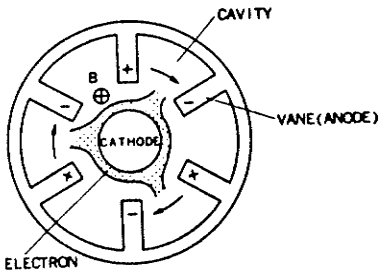

Figure 7.5 The Magnetron Interaction Space

The spokes of the electron cloud (Figure 7.5) tend to rotate about the cathode and when the angular velocity of these spokes synchronizes with the resonator frequency, the oscillation will be stably sustained. Essentially, the electrons serve to remove energy from the static electric field and transfer it to the microwave field.

7.2 Power Regulation

The magnetron operates in a pulsed mode, at a frequency of 60 Hz, in which the magnetron is on for roughly half a cycle, and off for the other half-cycle. The magnetron power supply (Figure 7.6) functions as a half wave rectifier and voltage doubler.

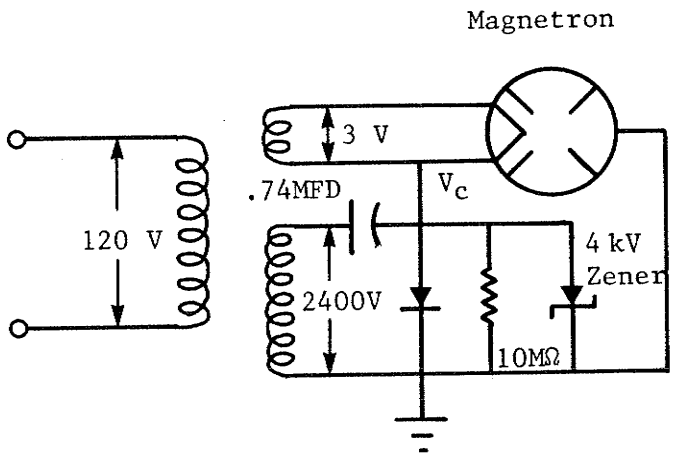

Figure 7.6 Magnetron Power Supply

The magnetron acts as a diode with a forward voltage of 4 kV and, therefore, clips the V_c waveform at -4 kV. The 4 kV zener diode protects the magnetron from transients and the 10 MΩ resistor discharges the capacitor when the power supply is turned off.

Since the microwave ion source will probably require less than 50 W of high frequency power, it will be necessary to operate the magnetron at a reduced power level, well below its rated 600 W output. This presents a problem since the microwave oven magnetron is designed for full power operation.

Two methods for controlling the output power, requiring only minor modifications to the power supply, were tested. The first method consisted of controlling the wave amplitude of the input voltage to the transformer by means of a variac. The idea was that as the amplitude of the input voltage is reduced, the 4 kV clipped portion of the cathode voltage waveform becomes narrower in width thereby decreasing the on-time of the magnetron and, hence, the average power.

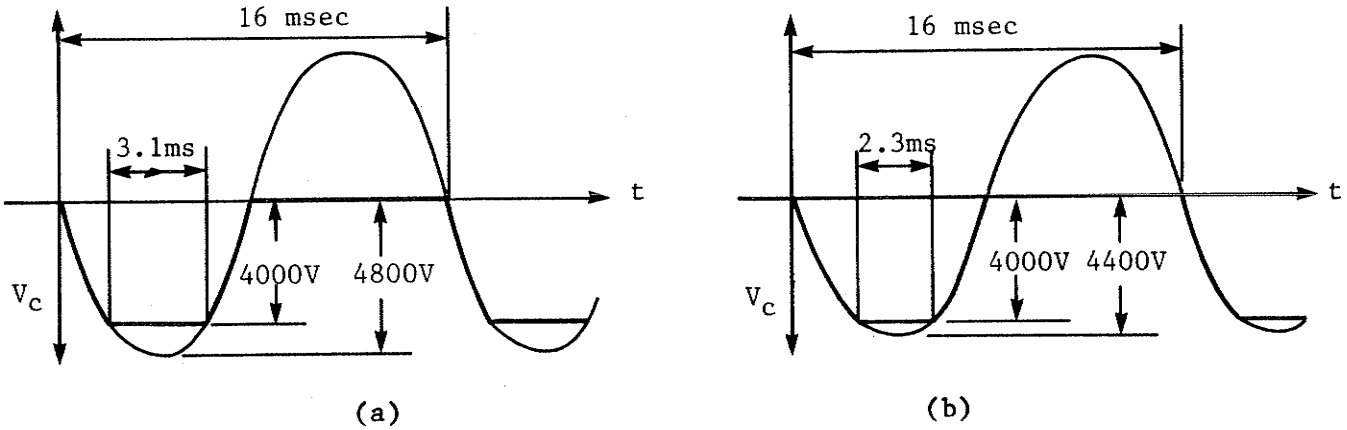

Figure 7.7 Voltage Waveforms

If, for example, the input voltage is reduced from 120 V (Figure 7.7a) to 110 V (Figure 7.7b), the amplitude of the clipped wave stays at -4 kV due to the regulating effect of the magnetron. The width of the clipped portion,

however, would have decreased from 3.1 msec to 2.3 msec. If the input voltage were further reduced to around 100 V, the width of the pulses would approach zero.

To test this technique, the magnetron was operated in the microwave oven from which it came. Vials of water placed in the oven cavity were heated and timed to the boiling point. The time it took the water to boil was used to gauge the power output of the magnetron.

It was found that adjusting the input voltage to the power supply did not have a significant effect on the power output of the magnetron. As the voltage was reduced from 120 V to 100 V, very little change in the power level (< 10%) was observed. At an input voltage of about 95 V, the magnetron stopped oscillating. The reason that this method was not effective may be that, when the magnetron is oscillating, it distorts the waveform so that it more closely resembles a square pulse than the waveform in Figure 7.7. In this case, the reasoning described in the preceding paragraphs is not applicable.

The second power control method that was tested incorporated a triac circuit (Figure 7.8) to reduce the input power to the magnetron.

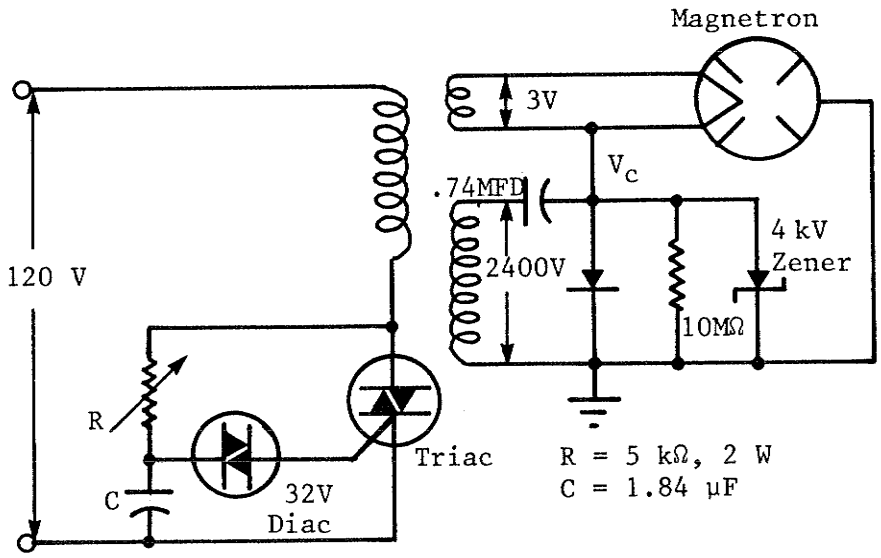

Figure 7.8 Power Supply With Triac

With the circuit of Figure 7.8 it is possible to cut off a portion of each half cycle of the input waveform (Figure 7.9).

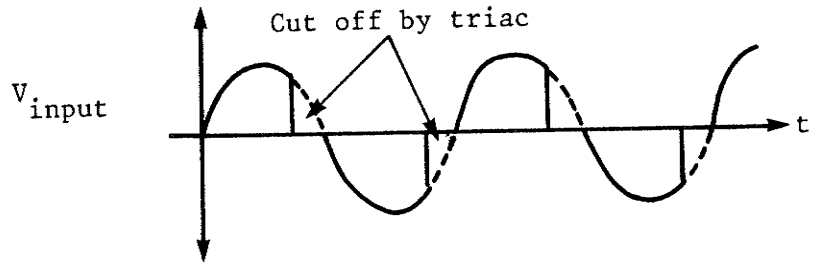

Figure 7.9 Effect Of Triac On Waveform

The variable resistor, R, controls how much of the waveform is cut off. It was thought that by removing part of the input wave, the width of the cathode voltage pulses would be reduced. Again, it was found that reducing the power input had little appreciable effect on the magnetron output, until a point was reached at which the magnetron stopped oscillating.

Figure 7.10 shows the voltage-current characteristics of a typical microwave oven magnetron.

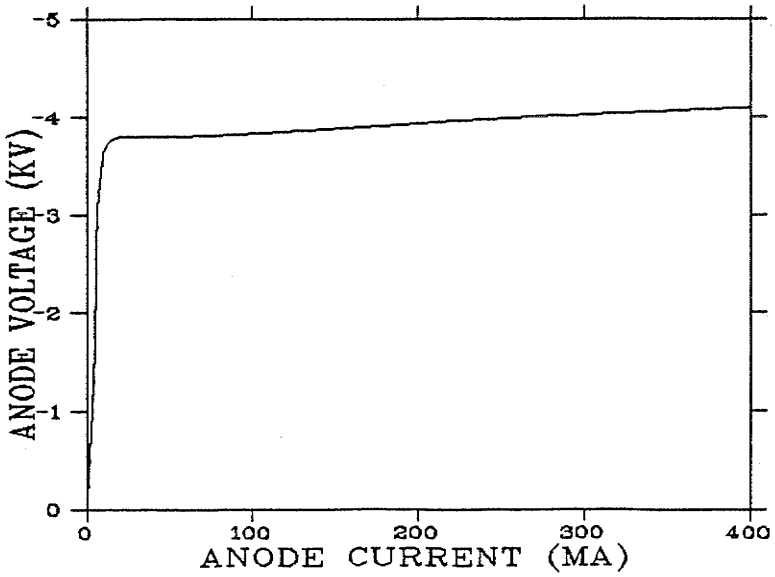

Figure 7.10 Voltage-Current Characteristics

It is seen that the anode voltage and current are linearly related over the operating range of the magnetron. In other words, as long as the magnetron is oscillating, its effective resistance R_m is constant. The anode voltage under oscillation conditions is therefore,

$$V_a = R_m I_a + V_o \qquad (7.2.1)$$

where V_o is the anode voltage at which oscillation sets in (from Figure 7.10, $V_o \simeq 3.8$ kV). Assuming a constant efficiency, η, over the entire operating range of the magnetron (η may actually vary by 5-10%), the microwave power delivered by the magnetron is

$$P = \eta V_a I_a \qquad (7.2.2)$$

Substituting equation (7.2.1) into (7.2.2) yields the following expression for power,

$$P = \eta R_m I_a^2 + \eta V_o I_a \quad . \qquad (7.2.3)$$

The magnetron power output is non-linearly related to the anode current, and by regulating the anode current, it should be possible to control the magnetron power level.

By replacing the part of the power supply that provides the cathode voltage with a current regulated dc supply (Figure 7.11), it should be possible to obtain precise power control of the magnetron.

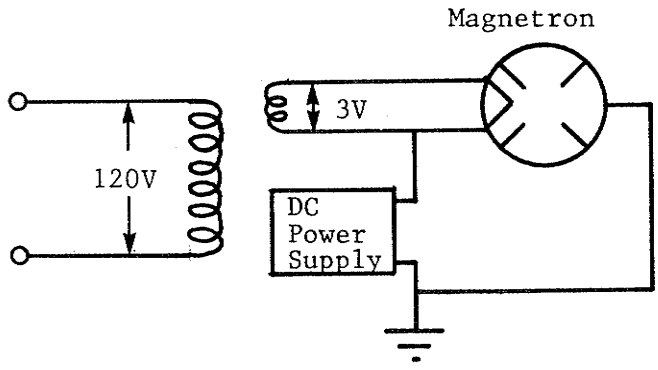

Figure 7.11 Magnetron Power Supply

By using a dc power supply to provide the anode current, the magnetron will no longer operate in a pulsed mode, but rather in a cw mode. From Figure 7.10, it should be noted that below an anode voltage of 3.8 kV and current of 20 mA, the magnetron will cease to oscillate. For a power efficiency of 50% (typical for a magnetron), this corresponds to a power of 38 W. This means that there exists a minimum power level below which the magnetron will not oscillate. It appears, however, that this minimum power level will fall below the actual power level ($\sim$ 50 W) at which the magnetron will be operating for the ion source.

7.3 Tuning the Microwave Source

The purpose of tuning the source is to find the operating conditions for which the power transfer to the plasma, and hence the beam current, is maximized. When the source is properly tuned, it is operational at its maximum efficiency and, therefore, consuming a minimum amount of power for a given beam current.

In the absence of any power meters, the simplest way to gauge the power absorbed by the plasma is by the beam current. For a given extraction voltage, the higher the beam current, the greater the energy absorbed by the plasma. This characteristic can be used to determine when the waveguide cavity is in resonance and when ECR is occurring. The following paragraphs describe a simple procedure for tuning the source.

First, apply a moderate extraction voltage (say 2 kV) to the probe electrode. This voltage will be maintained throughout the tuning procedure. Next, turn on the magnetron and set it to a power level slightly above the level at which it begins to oscillate. Take care to ensure that the microwave radiation near the source is at a safe level. Admit a small amount of

hydrogen to the source and gradually increase the gas pressure until a plasma ignites. A beam current should be observed.

At this point, the cavity can be tuned to resonance. Adjust the tuning plunger until the beam current is maximized. Next the solenoid magnet can be turned on. As the magnetic field is increased, the beam current will probably increase for a time and then steady out. This does not indicate the presence of ECR, but that the magnetic field is concentrating the plasma near the exit canal and is increasing electron lifetime. If the magnet current is further increased, the beam current should eventually begin to rise again as ECR sets in. The magnet current should be set so as to maximize the beam current.

The source, at this point, has been roughly tuned and the gas pressure should be adjusted so as to maximize the beam current. Changing the gas pressure will likely change the loading effect of the plasma to the degree that the source should be retuned. Actually, it may be found that tuning one parameter, such as the magnet current, may change the plasma characteristics sufficiently to throw the cavity out of resonance. It may be necessary to repeat the tuning procedure a number of times before each variable parameter converges to its optimum.

Once the source has been tuned, the magnetron power can be increased if necessary, but care should be taken to ensure that the source bottle is not overheated. The source should be forced air-cooled at all times during its operation. The only parameter that will be changed during normal operation of the source is the extraction probe voltage which controls the beam current. All other parameters should remain fixed at their optimum settings.

CHAPTER VIII

SUMMARY

The C-SO-164 is a radiofrequency ion source designed for use in a Van de Graaff accelerator. Operating at an RF frequency of 80 MHz, the maximum proton current attainable from the C-SO-164 was found to be less than one milliamp. The need for more intense beam currents has prompted a thorough investigation into the source's operating characteristics in an effort to understand and optimize its operation. In addition, a proposal and some general design criteria have been put forward for a modified version of the C-SO-164. It will employ microwave excitation with electron cyclotron resonance to produce more intense proton beams at a lower level of power consumption.

The first phase of the project involved the construction of a vacuum chamber test bed on which the C-SO-164 was mounted and its operating characteristics measured. The beam current and emittance were recorded over a wide range of probe voltages, magnetic fields, and hydrogen pressures. From these measurements, the following observations and conclusions were made:

1. The extracted beam current increases with probe voltage up to a peak value after which it begins to decrease. The decrease in current is due to the fact that, at higher extraction voltages, protons cannot be generated at the same rate at which they are removed. More electrons are removed from the plasma before they have a chance to collide, and, as a result, the ion production rate decreases causing a reduction in beam current.

2. The static magnetic field increases power transfer to the plasma by increasing electron lifetime and reducing recombination. It has the effect of concentrating the plasma around the center of the magnet near the exit canal. The general effect of the magnetic field on beam current is an initial increase in current up to a point after which increasing the magnetic field has no significant effect.

3. At low hydrogen pressures, a small peak in the beam current can be observed for a magnet current of 0.1 A corresponding to a field at the center of the magnet of $B = 3.82 \times 10^{-3}$ T. Since this field value is close to the field required for electron cyclotron resonance ($B_{ECR} = 2.86 \times 10^{-3}$ T), it is possible that the observed current peak is due to a small amount of ECR electron heating.

4. Increasing the hydrogen pressure causes a decrease in beam current. This is due to the increased recombination rate and reduced RF power transfer that occurs with increasing pressure. There does, in fact, exist an optimum pressure ($\nu = \omega$) for which the power transfer is maximized. At this pressure, the maximum beam current is also obtained.

5. The emittance of the C-SO-164 tends to decrease with increasing probe voltage. Increasing the probe voltage causes an increase in the axial velocities of the ions without affecting their transverse velocities. The result is a smaller divergence angle and, therefore, a lower emittance.

6. For a given ion energy, an increase in beam current produces an increase in emittance due to the effect of space charge blowup. At high beam currents, it is found that, due to the high ion concentration in the beam, the repulsive forces between ions cause a significant increase in the beam divergence.

7. For a given gas flow rate, the ionization efficiency is proportional to the extracted beam current. Assuming a pure proton current, the maximum ionization of the C-SO-164 was found to be 3.7%. The C-SO-164, like most simple RF ion sources, is only capable of ionizing a very small fraction of the gas molecules that enter the discharge. One of the objectives in converting the C-SO-164 to microwave operation is improvement of the ionization efficiency.

The modified version of the C-SO-164 will use a microwave oven magnetron with an operating frequency of 2.45 GHz to provide the high frequency power for generating the plasma. A short section of waveguide, with a WR-340 cross-section, forms a tunable resonant cavity in which the discharge is maintained. Only the TE_{10} mode is able to exist in the cavity, which produces an axial electric field in the source bottle. The magnetron output and the source bottle are located one half wavelength apart in the regions of peak electric field.

The magnet serves two functions. First of all, it concentrates the plasma near the exit canal, increasing both electron and ion lifetime. Secondly, the magnetic field can be used to induce electron cyclotron resonance. By the selective heating of electrons to high temperatures, ECR is able to greatly improve the efficiency of power transfer to the plasma without having a significant effect on the ion temperature.

It is expected that the modified version of the C-SO-164 will have microwave power requirements on the order of 50 W. In order to operate the magnetron at such low power levels, it will be necessary to replace the anode voltage power supply with a current regulated, high voltage, dc supply. By controlling the anode current, it should be possible to attain magnetron power

levels low enough to eliminate the risk of overheating the source bottle, or the magnetron itself.

The microwave version of the C-SO-164 should be well suited for operation in a Van de Graaff accelerator. It retains the favorable qualities of the RF source, which include ruggedness, simplicity, light weight, compactness, and no consumable electrodes. The additional anticipated advantages of the microwave source are an increased beam current capacity, a lower RF power consumption, and a higher ionization efficiency resulting in a lower gas consumption.

There is still a considerable amount of work left to do on the project, and its completion will be the subject of another thesis. Remaining work consists of completion of the resonator, winding of the solenoid, bench testing of the microwave source, and finally, installation of the source in the Van de Graaff accelerator.

REFERENCES

1. W.H. Rodebusch and W.C. Klingelhoeffer, J. AM. Chem. Soc. 55 (1933) 130.

2. P.C. Thoneman, Nature 158 (1946) 61.

3. P.C. Thoneman, J. Moofat, D. Roaf and J.H. Sanders, Proc. Phys. Soc. 61 (1948) 483.

4. A.J. Bayly and A.G. Ward, Can. J. Research A26 (1948) 69.

5. J.C. Ruthenglen and J.F.S. Cole, Nature 160 (1947) 545.

6. B. Koch and H. Neuert, Naturf 4a (1949) 452.

7. V.M. Mozerov, Dokl. AN SSSR 102 (1955) 61.

8. R.G. Wilson and G.R. Brewer, Ion Beams With Applications to Ion Implantation, (John Wiley & Sons, 1973) p. 65.

9. B.S. Marsicanin, Nucl. Inst. and Meth. 75 (1969) 106-108.

10. N.R. White, Nucl. Inst. and Meth. 206 (1983) 1-13.

11. W. Kuhlmann, J. Bojowald, C. Mayor-Boricke, J. Reich and A. Retz, Nucl. Inst. and Meth. 80 (1970) 89-94.

12. G. Doucas, H.R. McK. Hyder and A.B. Knox, Nucl. Inst. and Meth. 124 (1975) 11-22.

13. J. Vernon Smith Jr. and Paul Allison, Rev. Sci. Instrum. 53(4), 1982.

14. James H. Billen, Nucl. Inst. and Meth. 220 (1984) 225-250.

15. P.A. Reeve, L.P. Robertson, N.M. Al-Quazzaz and C.H.Q. Ingram, Nucl. Inst. and Meth. 114 (1974) 105-112.

16. Y. Wakuta, K. Matsuo and A. Nagao, Nucl. Inst. and Meth. 184 (1981) 583-585.

17. R. Geller, Appl. Phys. Letters 16 (1969) 401.

18. P. Apard, S. Bliman and R. Geller, Nucl. Inst. and Meth. 129 (1975) 357-363.

19. R. Geller, IEEE Trans. on Nucl. Sci. NS-23(2) (1976) 904-912.

20. J. Arianer and R. Geller, Annu. Rev. Nucl. Sci. 31(2) (1981) 19-51.

21. R. Geller, B. Jacquot and R. Pauthenet, Rev. Phys. Appl. 15 (1980) 995.

22. Y. Jongen and R. Ryckewaert, IEEE Trans. on Nucl. Sci. NS-30(4) (1983) 2685-2689.

23. Y. Sakamoto, Proc. Symp. Eng. Probl. Fusion Res. CH1441-5 (1979) 673-675.

24. J. Ishikawa, Y. Takeiri and T. Takagi, Proc. Int'l Ion Engineering Congress - IPAT'83 Kyoto (1983) 379-384.

25. A.J. Borden Fuller, Microwaves, (Pergamon Press, 1969) p. 178.

26. K. Bernhardi, G. Fuchs, M.A. Goldman, H.C. Herbert, W. Walcher and K. Wiesemann, IEEE Trans. on Nucl. Sci. NS-23(2) (1976) 999.

27. A.J. Lichtenberg and M.A. Liebermann, Plasma Phys. 15 (1973) 125.

28. F.C. Feshenfeld, K.M. Evenson and H.P. Broida, Rev. Sic. Instr. 36(3) (1965) 294-298.

Textbooks and General References Used in the Preparations of this Thesis

T1. L. Valyi, Atom and Ion Sources, (John Wiley & Sons, 1977).

T2. A.J. Borden Fuller, Microwaves, (Pergamon Press, 1969).

T3. R.G. Wilson and G.R. Brewer, Ion Beams with Applications to Ion Implantation, (John Wiley & Sons, 1973).

T4. Ion Implantation Techniques, from the Springer Series in Electophysics, Vol. 10, ed. H. Ryssel and H. Glawischnig, Springer-Verlag Berlin Heidelberg, New York, 1982.

T5. John D. Krauss and Keith Carver, Electromagnetics, McGraw-Hill Book Co., New York, 1973.

APPENDIX A

Trigger Circuit and Current to Voltage Convertor

TRIGGER CIRCUIT

The trigger circuit is designed to sense the negative edge of the noisy voltage pulse that comes from the scanner microswitch and to emit a negative TTL pulse of 500 nsec width for triggering the HP3456 programmable voltmeter. After detecting a single trigger pulse, the circuit locks out all subsequent trigger pulses until the circuit is manually reset.

The signal from the microswitch is directed to the non-inverting input of the LM-311 comparator which compares it with a small reference voltage set by the 100 kΩ potentiometer. This reference voltage is set so that the LM-311 will not trigger on low amplitude noise. The 47 kΩ resistor between the input and ground prevents the comparator input from floating when the microswitch is in the open position.

The microswitch bounce is filtered out by the 20 kΩ resistor and 1 uF capacitor at the output of the comparator. When the scanner microswitch is closed, a signal level of $\sim$ 1 V is applied to the input of the comparator causing the comparator output to swing to 5 V. When the microswitch is opened again, the comparator output drops down to a logic 0. The 7474 D flip-flop, which is triggered on a falling edge, clocks a logic 1 though to the Q output. The 74123 nonstable multivibrator is configured as a one shot, triggered on a rising edge. When the flip-flop output goes high, the 74123 is triggered and emits a negative pulse of 500 nsec width. This pulse is fed to the trigger input of the HP3456.

Once the D flip-flop has been triggered, any further clock pulses will have no effect until the flip-flop is cleared by pushing the reset switch.

Figure A.2 shows the current to voltage converter that was used to measure the current picked up by the rotating scanner. It has a sensitivity of 1.0 V output for 10.0 μA input.

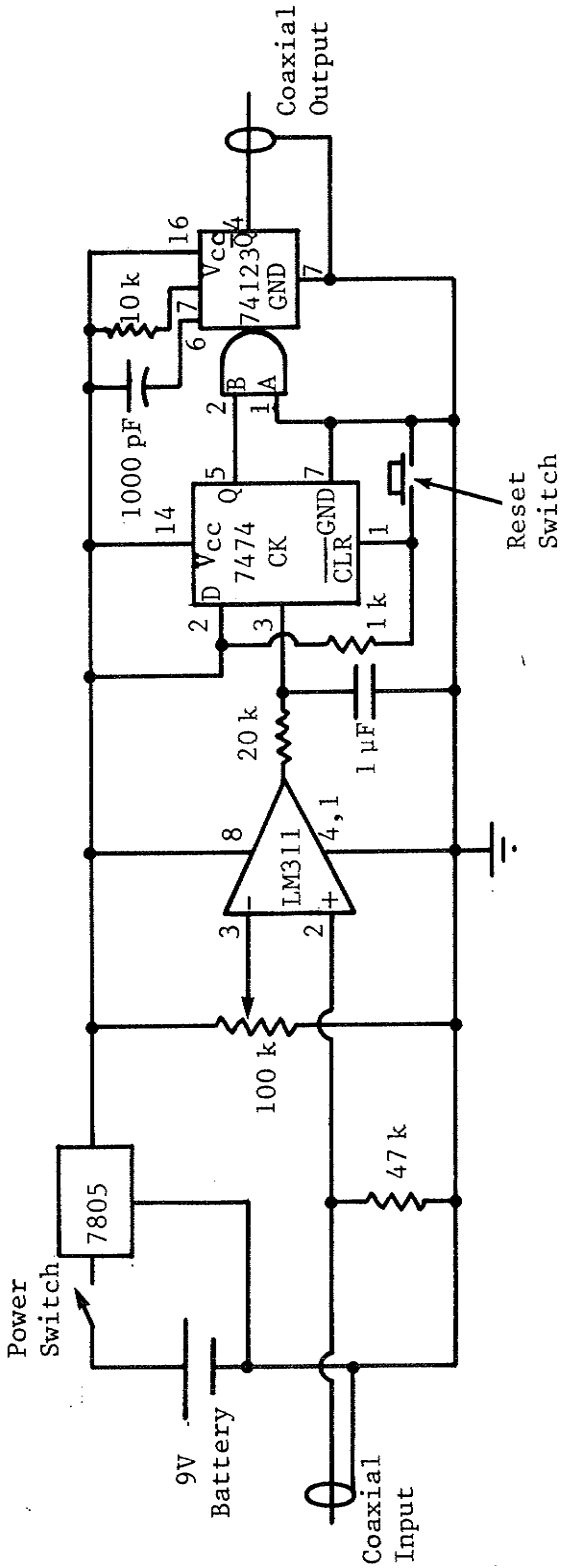

Figure A.1 The Trigger Circuit

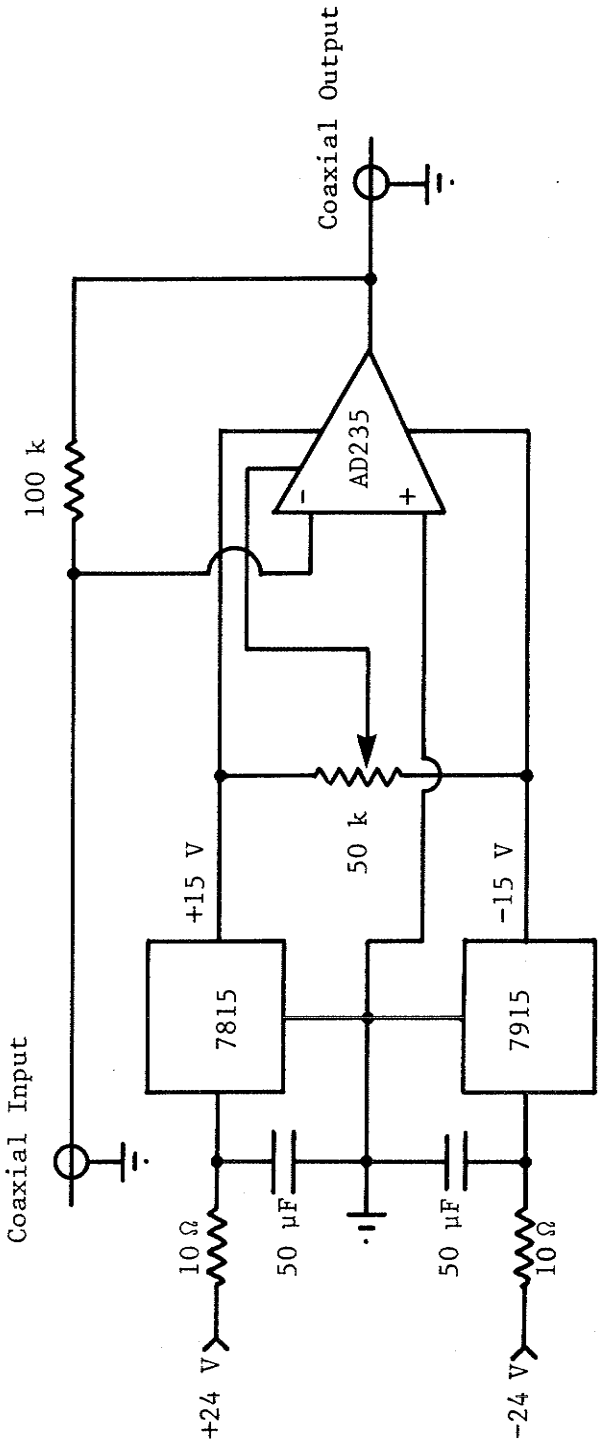

Figure A.2 Current to Voltage Converter

APPENDIX B

C-SO-164 Emittance Contours

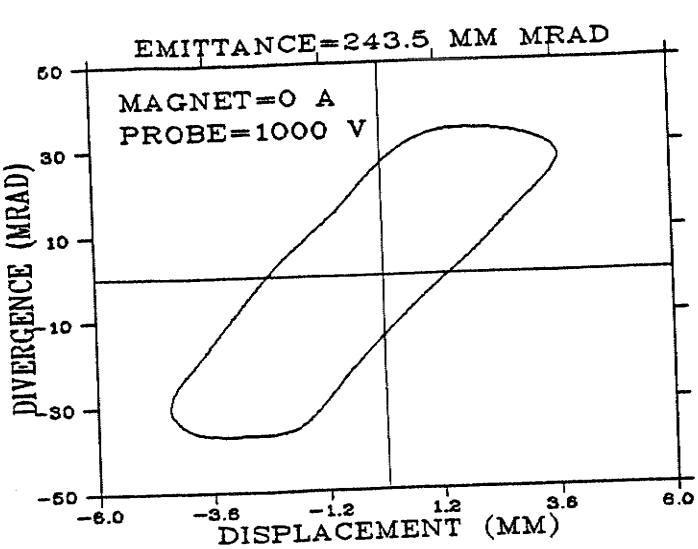

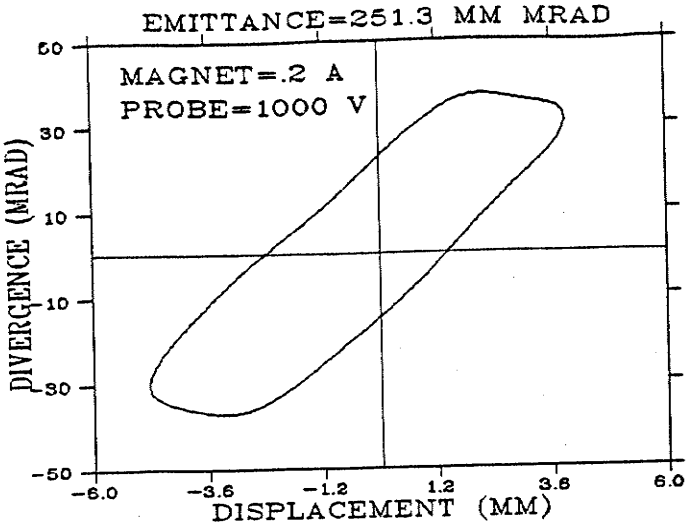

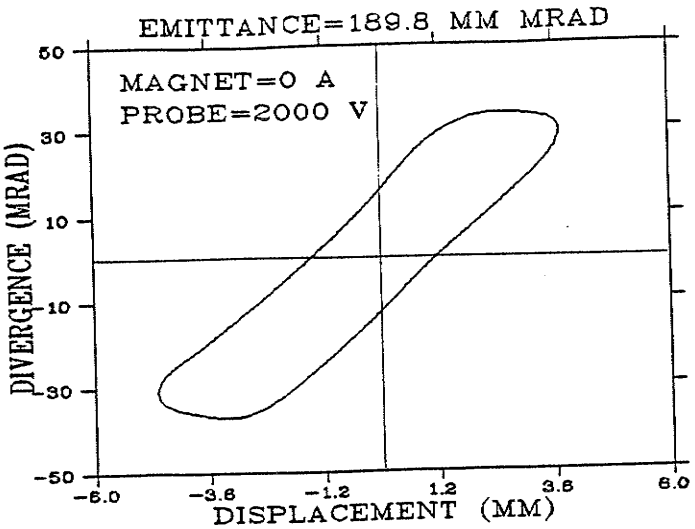

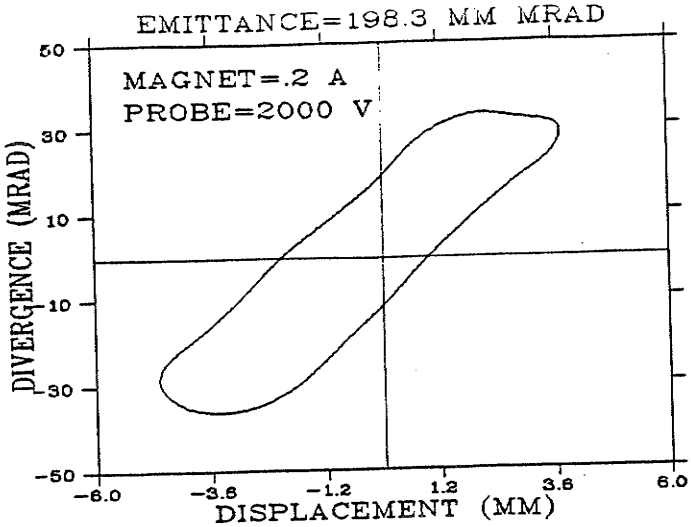

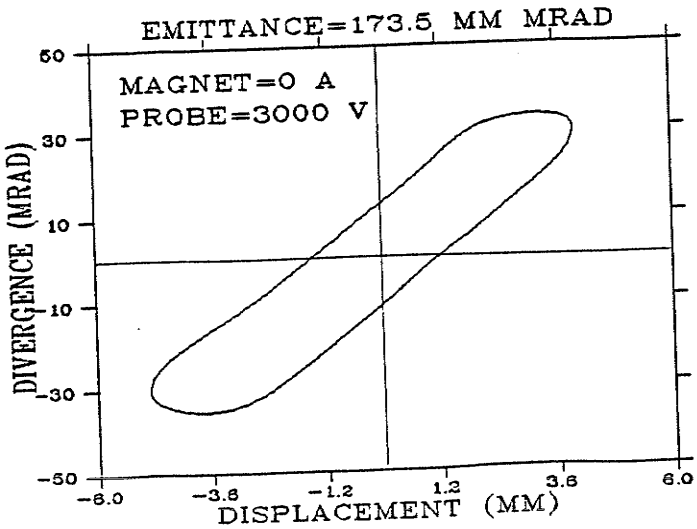

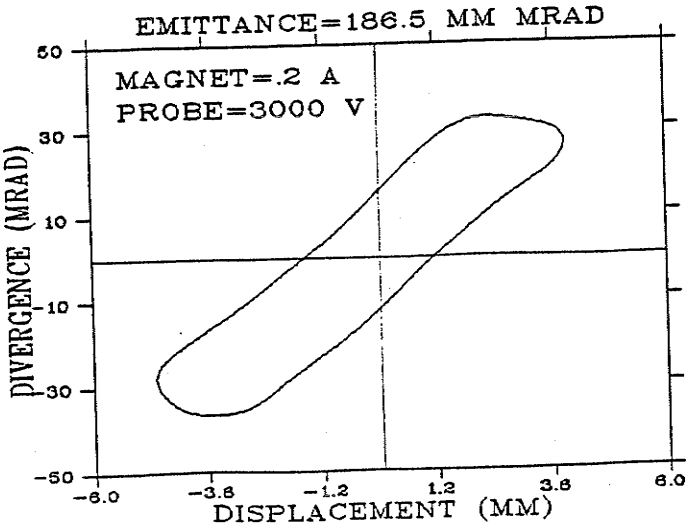

Horizontal Emittance

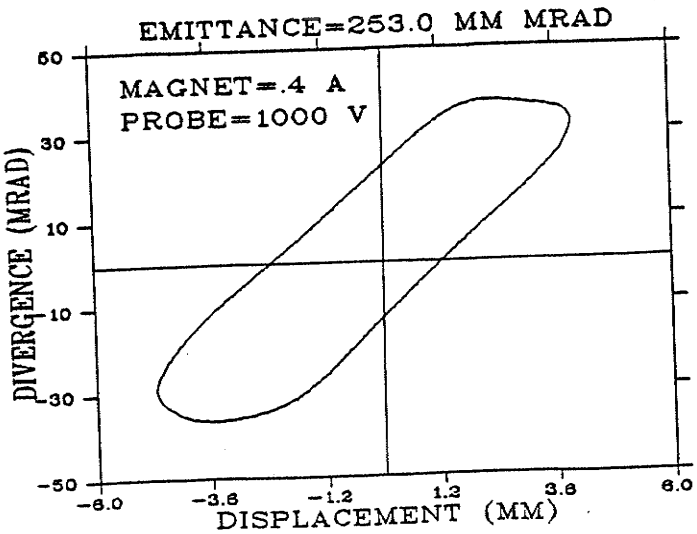

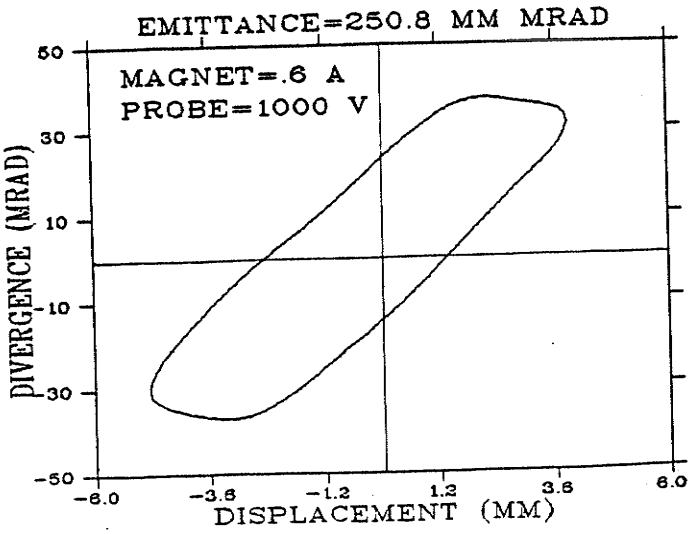

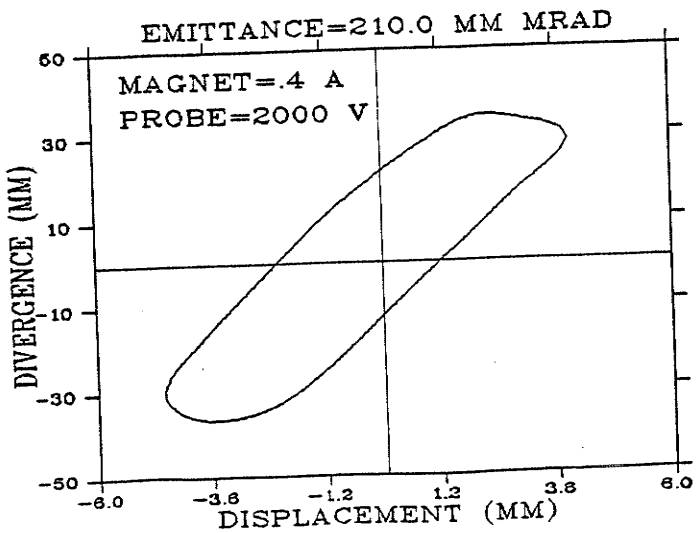

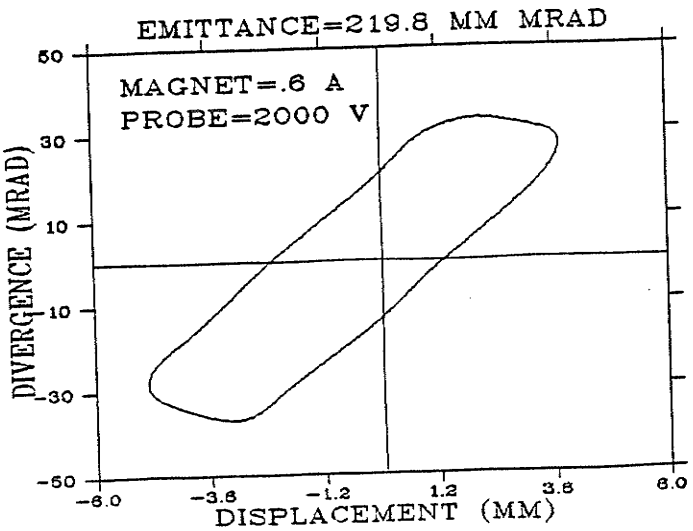

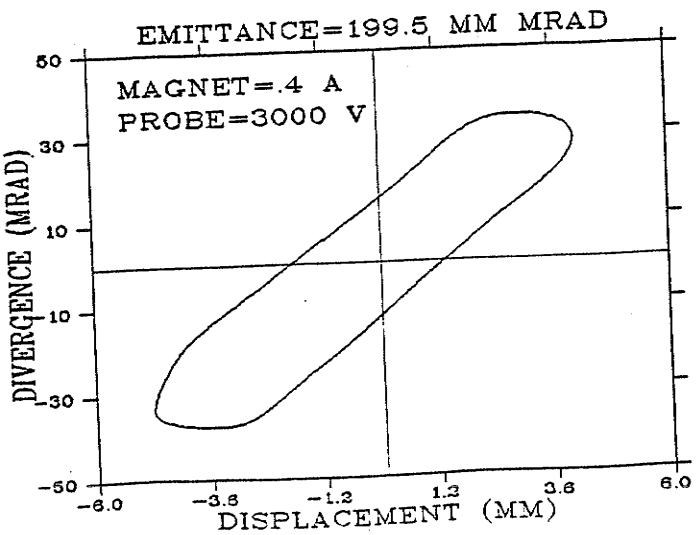

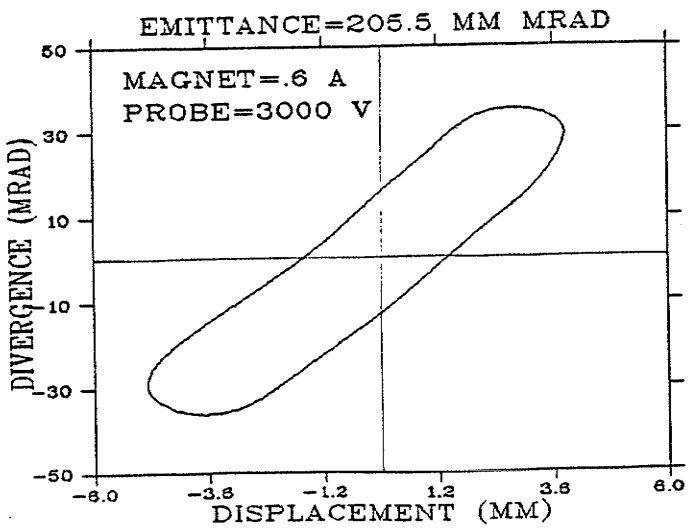

Horizontal Emittance

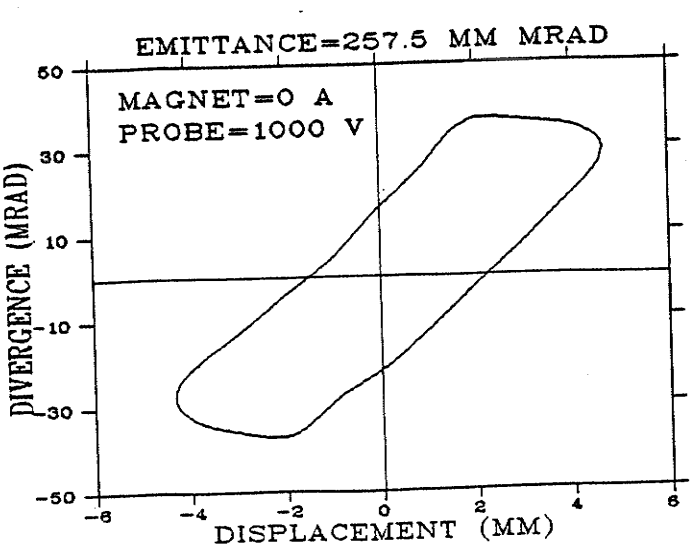

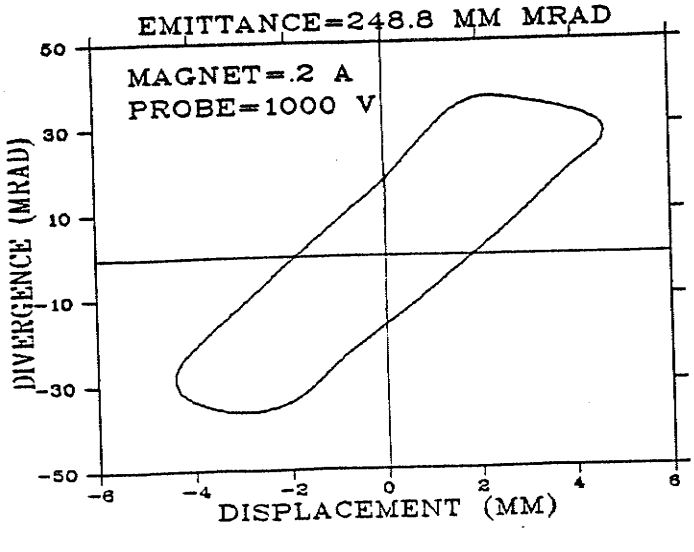

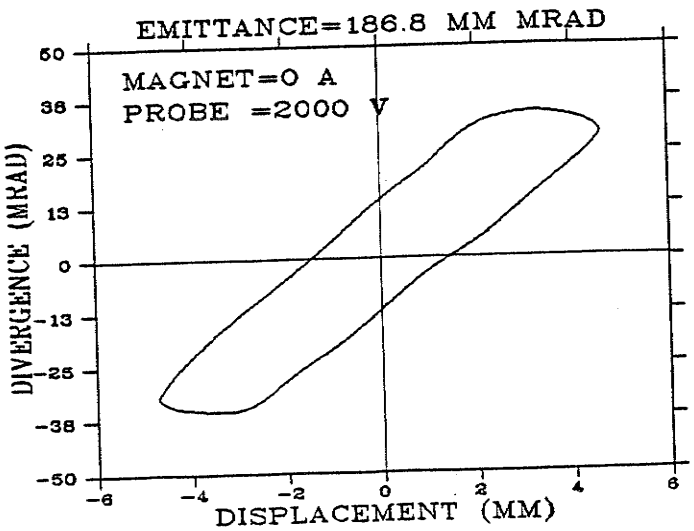

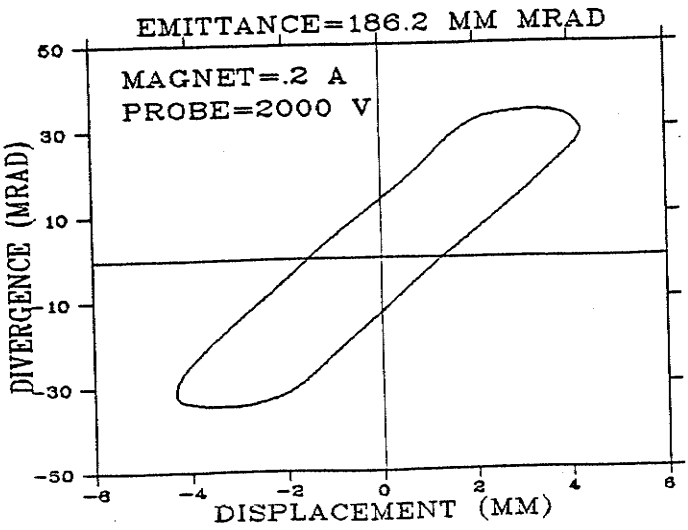

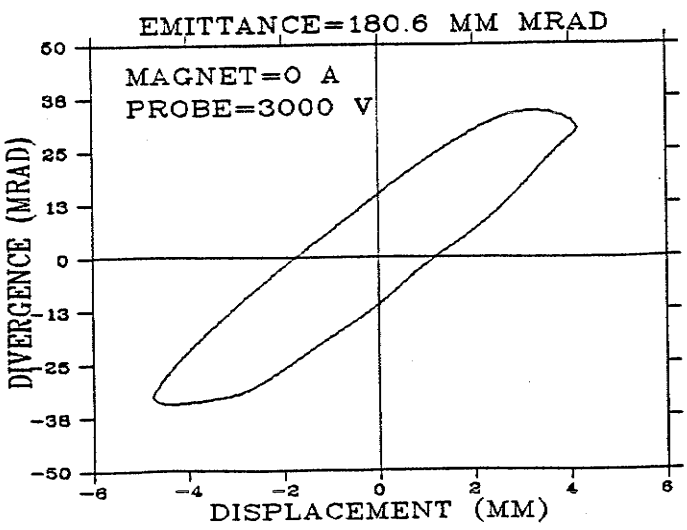

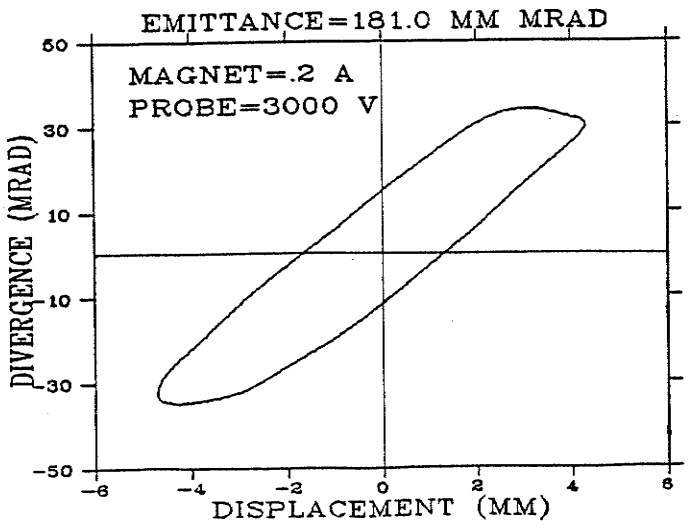

Vertical Emittance

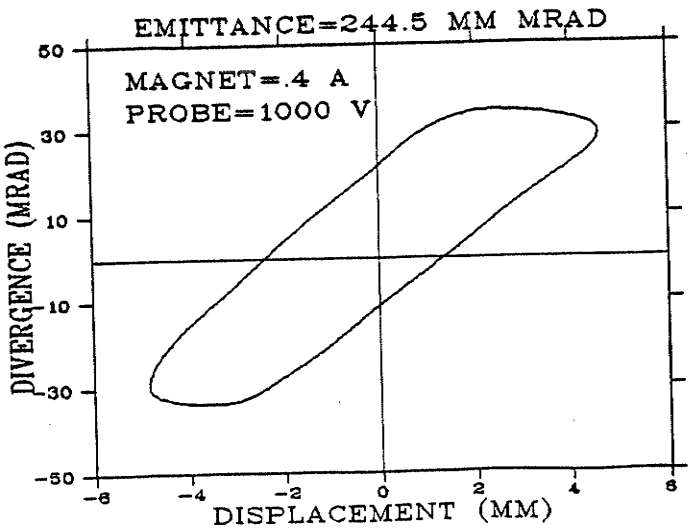

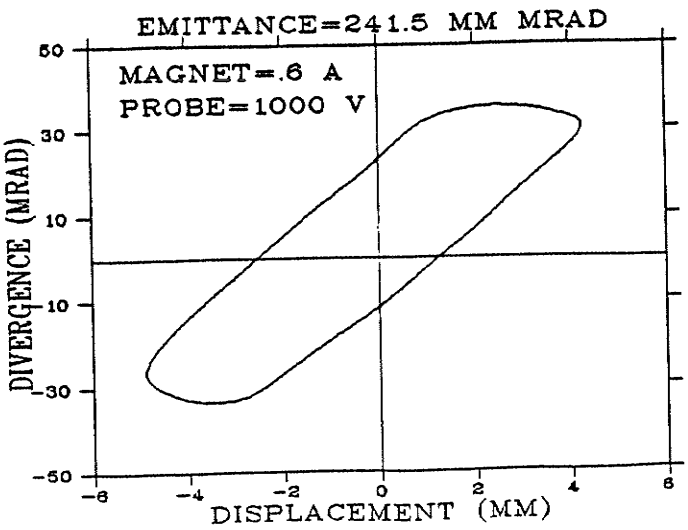

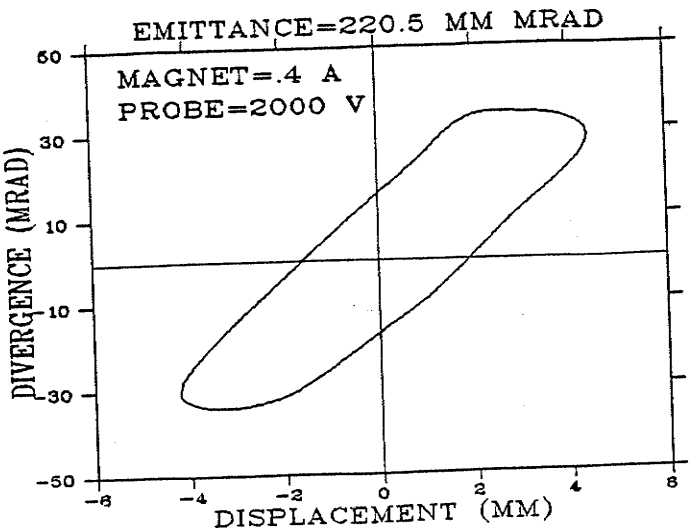

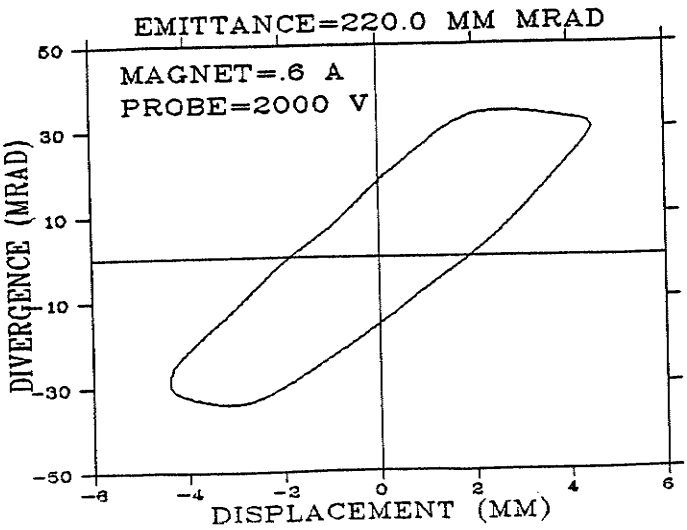

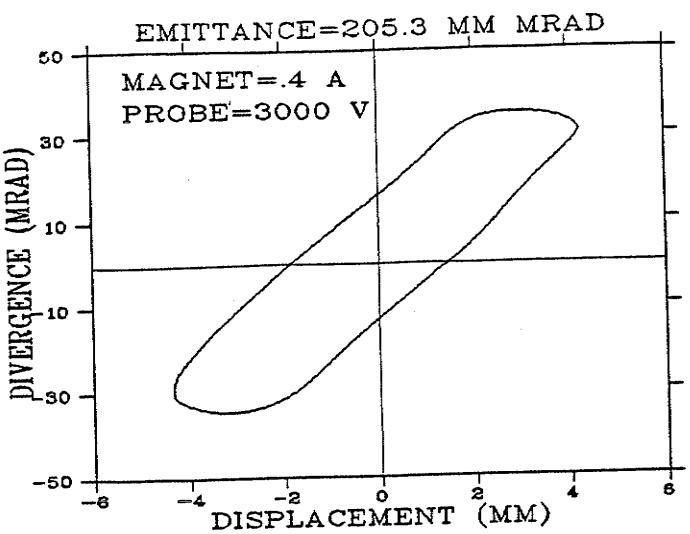

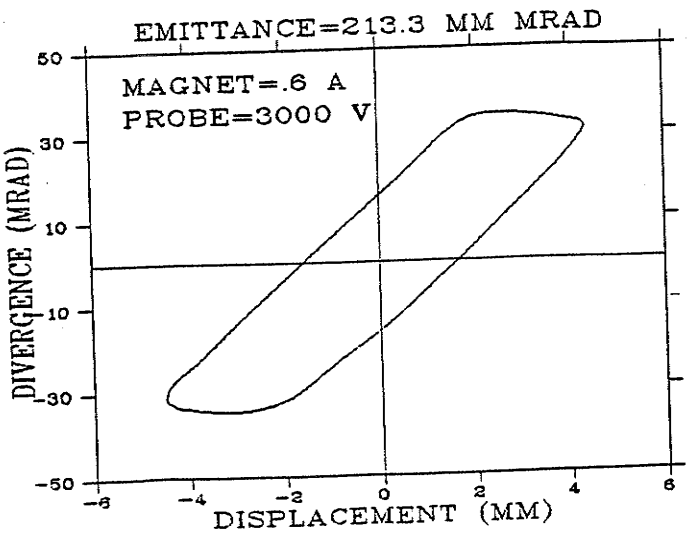

Vertical Emittance

APPENDIX C

Resonator Details

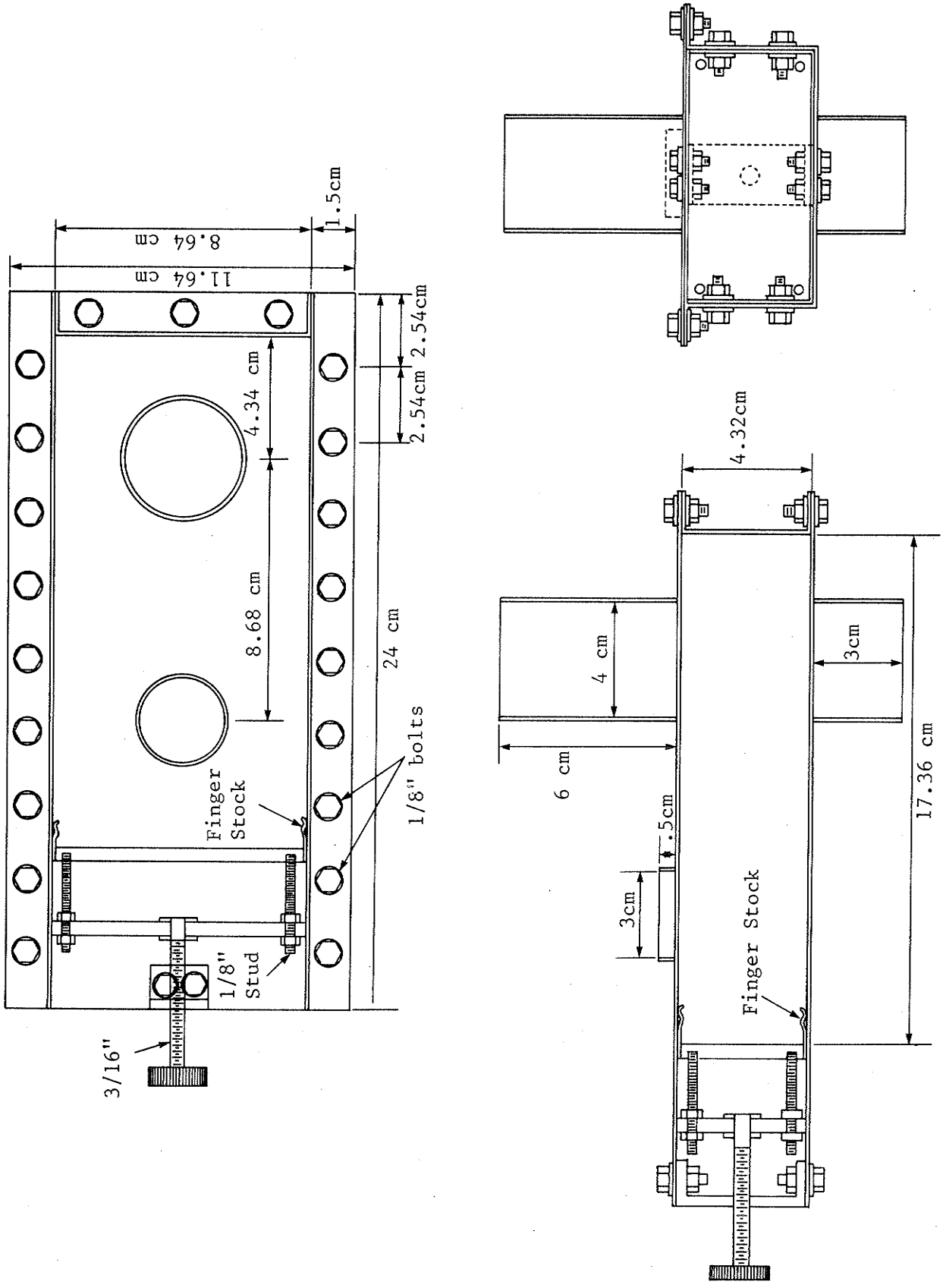

Figure C.1 Resonator Details